S.E. van Doorn

Date: 18 March 2020

The underlying processes of evaporative changes

within the transition period in the Miombo Woodlands, Mpika, Zambia in 2018

TU Delft

The underlying processes of evaporative changes

Within the transition period in the Miombo Woodlands, Mpika, Zambia in 2018

By

S.E. van Doorn

in partial fulfilment of the requirements for the degree of

Master of Science
in Civil Engineering

at the Delft University of Technology,
to be defended publicly on Tuesday March 24, 2020 at 02:00 PM.

Supervisor:	Dr. Ir. A. M. J. Coenders	TU Delft
Thesis committee:	MSc. C.D. Jimenez Rodriguez,	TU Delft
	Dr. B. M. van Breukelen	TU Delft

TU Delft

Preface

This report is part of the evaporation team of the ZAMSECUR project at the start of the project. The goal is to measure the evaporation within the Luangwa Basin in which a lot of Miombo Woodlands is found. I would like to thank the TU Delft for making it possible to go to Zambia and learn about doing fieldwork with limited resources. Besides I would like to thank Z. Su and L. Wang of the University Twente for providing the required SEBS evaporation data. Moreover, I would like to thank my supervisors for their guidance and the people of the University of Zambia (UNZA) for their hospitality and their local knowledge.

Summary

The Miombo woodlands are characterized by a transition period which is defined as the dry period in which grasses wither, trees shed and flush their leaves a few weeks before the rainy season. It is difficult to measure evaporation, due to the influence of the plant water storage on the water availability during the dry season. The seasonal variation in the plant water storage makes it even harder, as the time lag between the plant water storage and the terrestrial groundwater storage varies between the 0 to 90 days depending on the vegetation density. (Tian et al., 2018). It is unclear why the trees prefer this early flushing strategy and what is triggering the shedding of old leaves and flushing of new leaves. It is, however, difficult to remotely sense the variation during this period.

In this report, the outputs of several evaporation products and the vegetation indices are studied and compared to see how well the models follow the transition period. The three models, that are chosen for the comparison use different methods to indirectly calculate the evaporation flux. The first model is the Surface Energy Balance System (SEBS), which is based on the Surface Energy Balance as the name suggests and calculates the evaporation through land-atmosphere relationships. The second model is the Global Land Evaporation Amsterdam Model (GLEAM); this model uses the water balance model to calculate the water stress factor, which reduces the potential evaporation to calculate the actual evaporation. And lastly, the MODIS Terrestrial Evapotranspiration (MOD16A2) is looked into as this model uses the Penman-Monteith equation as a basis to separately calculate the evaporative fluxes such as transpiration, soil evaporation, and interception.

The outputs of the evaporation models differ quite a lot especially during the transition period. This is among other things due to the input variable such as vegetation indices. There are several vegetation indices such as the Normalized Difference Vegetation Index (NDVI), the Normalized Difference Infrared Index (NDII) and the Leaf Area Index (LAI). The difference in the indexes, however, is minimal and only small timing difference can be found. This means that the output differences are not influenced by the vegetation indices.

If the trends of the vegetation indices are compared with study observations and the evaporation models, it can be concluded that MODIS seems to follow the vegetation indices the most. GLEAM overestimates the water stress as the model does not react to the transition period at all. This is probably because GLEAM is based on the water balance and the root zone defined by the model is too small. Moreover, the model doesn't take into account the plant water storage which is a mechanism that should reduce the water stress that the trees experience.

SEBS on the other hand seems to respond well until the start of July in which the model starts to oscillate. The oscillations could be due to the slash and burn culture which happens around this time. Due to the dependency on temperature and radiation values, SEBS can be more strongly affected by the slash and burn culture than the other two models. The model is, therefore, not suitable to map the transition period as it constantly overestimates the evaporation and the data oscillates.

Lastly, MODIS seems to agree with the output of the vegetation indices which the model follows quite well. The MODIS output is, however, averaged over several days and due to these daily variations can be lost. Besides if the vegetation indices are unable to capture the transition period, the MODIS output will wrongly estimate the evaporation. As this research is based on mostly satellite images supplemented by field observations, no statements can be made about it how accurate the models are. But based on this research, the MODIS model seems to be the preferred evaporation output. And as the evaporation output for some of the models can be twice or even three times as big, the choice of model can have a big impact on your evaporation values.

Table of contents

Parameter definitions

A	=Rn
A_c	part of the net radiation allocated to the canopy
A'	available energy for H and λE
A_{soil}	the part of A partitioned to the soil surface
α	albedo (SEBS)
α	Priestley and Talyor coefficient (-) (GLEAM)
C_p	specific heat of air at constant pressure
Δ	the rate of change of saturation vapour pressure with temperature (kPa/K)
e	actual vapour pressure
e_s	saturation vapour pressure (or e_{sat})
ε	emmisivity of the surface (MODIS)
λE	latent heat flux (λ = latent heat of vaporization (MJ/kg), E = actual evapotranspitation (mm/d))
λE_p	latent heat flux (λ = latent heat of vaporization (MJ/kg), E_p = potential evapotranspitation (mm/d))
$E_{i-1}^{(l)}$	Evaporative flux of the previous day (mm/d)
$F_{s,i}^{(l-1)}$	Slow draining flux into the layer (mm/d)
$F_{f,i}^{(l-1)}$	Fast draining flux into the layer (mm/d)
$F_{s,i}^{(l)}$	slow draining flux out of the layer (mm/d)
F_c	fractional canopy coverage
F_{wet}	water cover fraction
G_0	soil heat flux (W/m^2)
H	sensible heat flux
H_{wet}	sensible heat flux under wet conditions
H_{dry}	sensible heat flux under dry conditions
λ	latent heat of vaporization
LAI	Leaf Area index
NDVI	Normalized Difference Vegetation index
NDII	Normalized Difference Infrared index
ρ	density of air
P_a	atmospheric pressure
M_a	molcular masses of dry air
M_w	molecular masses of wet air
p_d	fraction rain to trunks
R_n	net radiation (W/m^2)
RH	Relative humidity
rhrc	aerodynamic resistance
rrc	resistance to radiative heat transfer
r_e	external or aerodynamic resistance
r_a	aerodynamic resistance
r_s	surface resistance
r_{as}	aerodynamic resistance at the soil surface
r_{tot}	total earodynamics resistance
Λ	relative evaporation
Λ_r	evaporative fraction
s	the slope of the curve relating saturated water vapour pressure to temperature
S	Stress factor
VOD	Vertical Optical Depth
VPD	air vapour pressure deficit

ψ	the psychometric constant (kPa/K)
$\omega_i^{(l)}$	Water content (m^3/m^3)
ω_{wp}	Water content at wilting point
ω_p	porosity of the soil matrix
ω_r	the residual soil moisture
γ	psychrometric constant

1. Introduction

Evaporation during the transition period in the Miombo Woodlands is hard to measure due to the influence of the plant water storage on the water availability during the dry season which makes it possible for trees to flush their leaves at the end of the dry season (Tian et al, 2018). This early flushing of young leaves is also called pre-rain leaf emergence or green-up and is part of the transition period which occurs in the Miombo Woodlands. The transition period starts at the start of the dry season in which grasses start to wither and end with the flush of new grasses with the next rainy season. In between, the trees shed their leaves and flush them again. The exact timing of this shedding and flushing, however, varies for each tree species in time and space (Ryan et al., 2017).

It is unclear why the trees are doing this and what is triggering the trees to start shedding and flushing their leaves. According to Chidumayo and Frost (1996), the shedding time is dependent on the weather conditions in the previous rainy season as the leaves shed early in years with below-average rainfall and the reverse in years with above-average rainfall. The timing of the green-up is, however, well synchronized within a species with only a small difference of trees growing on shallow and deeper soils. (Chidumayo and Frost, 1996).

The purpose of this report is to test how accurate evaporation models that differ in theoretical basis will represent the transition period in the Miombo woodlands. The Miombo woodlands have due to the heterogeneity and the transition period a very complex ecosystem. While conventional field techniques to measure evaporation are relatively accurate in estimating the evaporation over homogenous areas, the techniques are limited for large-scale terrain areas as they have to be extrapolated/interpolated to various temporal and spatial scales. Due to these limitations the remotely sensed data is seen as the only viable technology to map evaporation over larger areas. (Li et al, 2009)

The main problem for satellite in this type of ecosystems, however, is the niche separation of trees and grasses which have to be captured in an integrated signal of both. (Higgins et al., 2011) According to Tian et al. (2018), remotely sensed data had difficulty sensing the seasonal variation in plant water storage for tropical woodlands such as Miombo Woodlands. The study found that the time lag between the plant water storage (L-VOD) and terrestrial groundwater storage (TWS) varies between the 0 and 90 days depending on the vegetation density. As denser vegetations increase the time lag. This also indicates a different role between the trees and the understory which consists of herbaceous plants and shrubs. (Tian et al., 2018)

Several types of evaporation models are available and it is unclear how well those models react to the rapid changes in vegetation during the transition period. As such, a small plot of Miombo woodlands located in Kalonje, Mpika District, Muchinga Province in Zambia will be studied to determine the accuracy of the evaporation models and the vegetation indices that they are based on. This area is chosen as it is representative of the wet Miombo woodlands in the Luangwa Basin. In addition, due to the field plot being fenced in the period from August to December, the plot is not disturbed during the transition period and is left unburned.

The report will start with a definition of the vegetation stages within the study site as this will be the starting point of further analysis. This definition will be based on a combination of in-situ measurements and observation of the visual spectrum of the Sentinel-2 imagery. Afterward, the evaporation products including the Surface Energy Balance System (SEBS), the Global Land Evaporation Amsterdam Model (GLEAM) and the MODIS terrestrial evapotranspiration model will be reviewed while keeping in mind the vegetation index that has been used as an input. In the end this should give us a clear overview of the timing and the effect of the transition period on the evaporation within the wet Miombo woodlands in Mpika.

2. Methodology

2.1 Site description

The study site is located in the Zambezi river basin, which is the fourth largest basin of Africa (Frenken en Faurès, 1997), and more specifically in the Luangwa river basin. The Luangwa River has a unique location as it is located between the Kariba and Cahora Bassa dams and influences the flows towards the dams and thus the flow regulations of the dams. Besides, the Luangwa River is the largest tributary between the dams with a mean annual discharge of 518 m^3/s (World Bank, 2010). It is, however, hard to predict flows from the Luangwa river as it is largely ungauged. Because of this, the evaporation is measured to understand how much water is left within the delta.

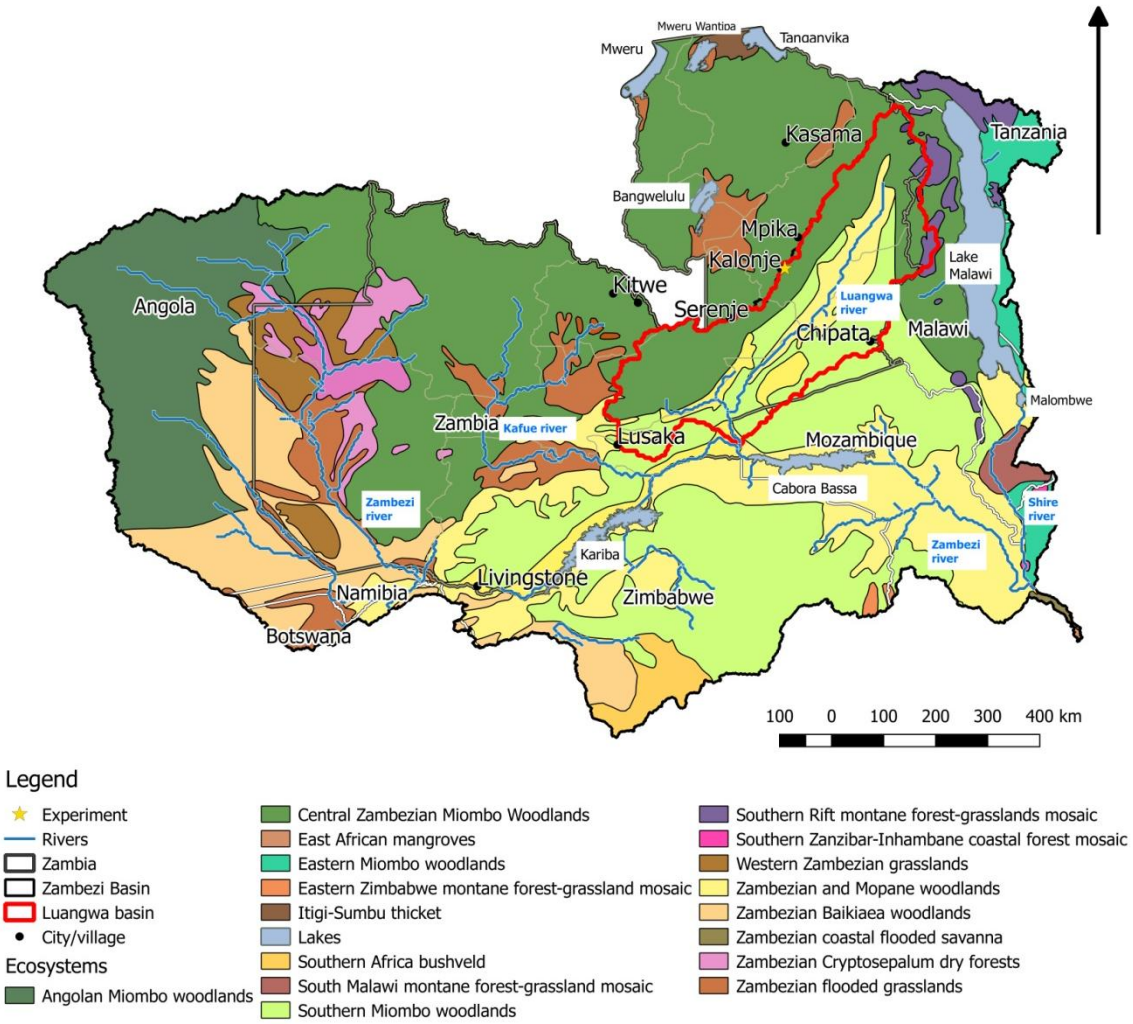

Figure 1 Vegetation throughout the Zambezi river basin and Zambia (the map is based on information from Lehner et al. (2006); FAO-UN-AGLW (2000); MapCruzin (2019); © 2018- GADM; Olsen et al., 2001)

The field work site is put in one of the main vegetation types of the Luangwa river basin in this case the Miombo Woodlands. There are two types of Miombo woodlands in the Luangwa Basin which are Central Zambezian Miombo Woodlands and Southern Miombo Woodlands. The two types are distinguished by the annual rainfall amount. The Central Zambezian Miombo Woodlands has an annual rainfall of above 1000 mm/year and the Southern Miombo woodlands of less than 1000 mm/year. (Olsen et al., 2001) As the wet Miombo woodlands have a higher amount of rainfall, this Miombo type is chosen for the field site.

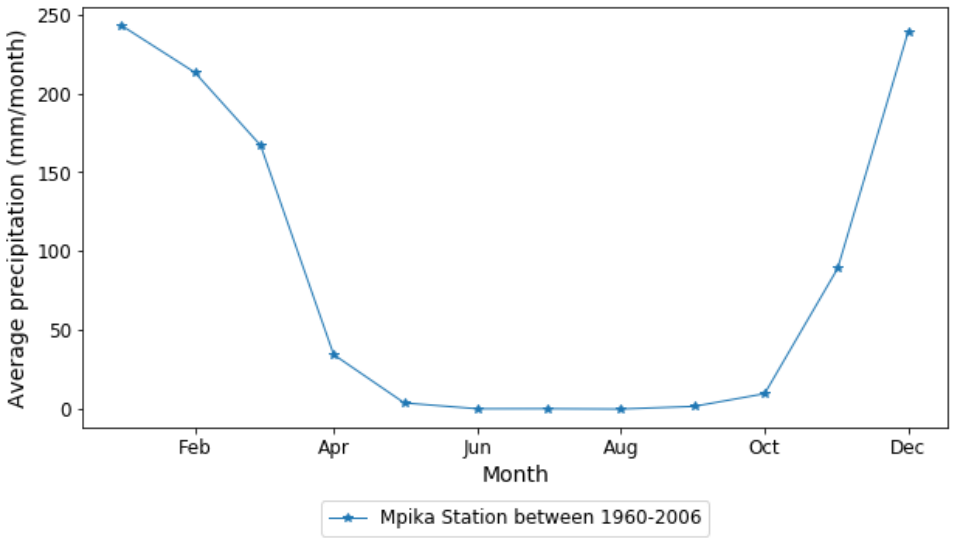

Figure 2 Monthly precipitation at Mpika Station (Zambian Meteorological Department, 2019)

The weather is the basin is influenced by the Inter-Tropical Convergence (ITCZ) which migrates southwards during the summer. The southwards movement will bring the ITCZ above the Northeast of Zambia. The ITCZ converges several moisture inflows such as the monsoonal flow from the Indian Ocean and the cyclonic flow emanating from the Atlantic over central Zambia. (Hachigonta and Reason, 2006). Therefore, the wet season is from November to March and the dry season is from April to October as also shown by the Mpika Weather station (2019) in Figure 2. This station is located about 60 km from the site and latitudinal and longitudinal coordinates 11.9 °S and 31.4 °E. According to the available data of the Zambian Meteorological Department of 1960-2006, the rainfall at the Mpika Weather station is often between the 850 – 1150 mm per year.

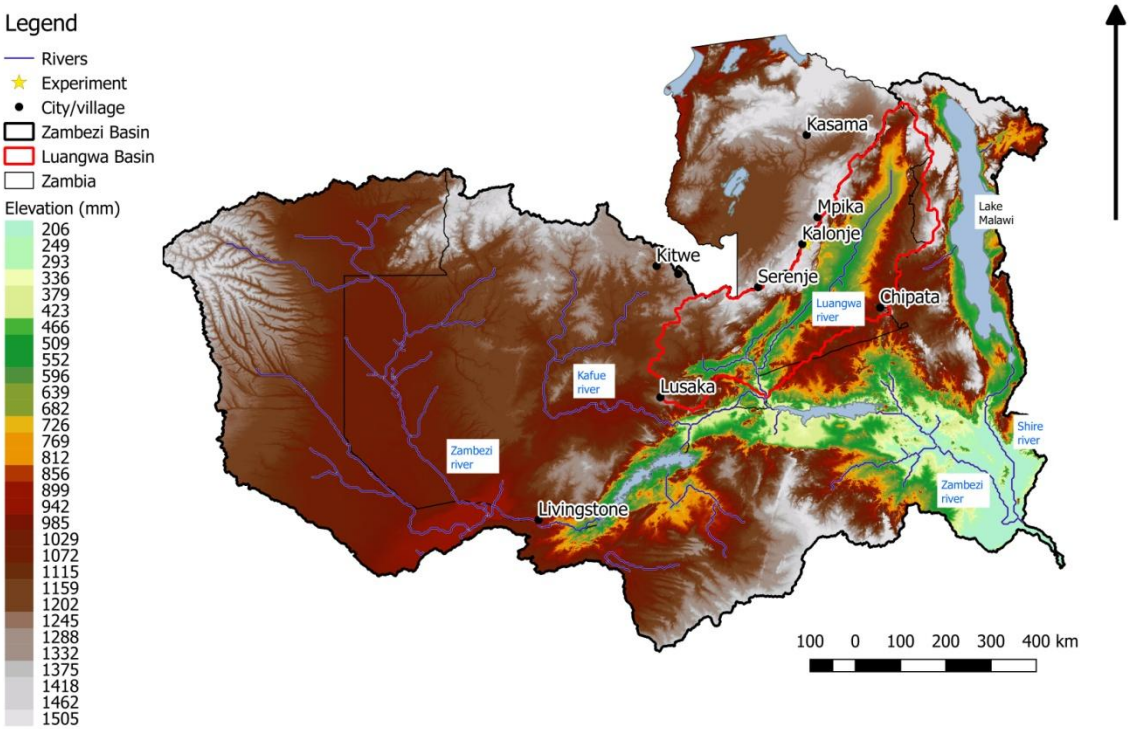

Figure 3 Elevation in the Zambezi Basin and Zambia (map based on data of Lehner et al. (2008))

Elevation

As mentioned above, the study site is located in the Miombo Woodlands which is a very common tropical seasonal woodland in Southern Africa as it covers about 2.7 million km^2. (Frost, 1996; Gumbo et al., 2018) The Woodlands are mostly located on the higher elevated areas of the Luangwa Basin as shown in the comparison between Figures 1 and 3. Moreover, it is shown that the study site is located on a plateau with very steep slopes between the plateau and the valley, also called the Muchinga escarpments. On the plateau itself, the woodlands are interrupted by lower laying seasonally inundated wetland areas. (Heyden and New, 2003).

These wetland areas are also called dambos and can stretch over several kilometers but the width is no more than a few hundred meters. (Chidumayo, 1992) Especially in high rainfall areas such as the area around the study site, the dambos are quite extensive. A distinction can be made between wet and dry dambos based on the water table throughout the year. Wet dambos have a water table near, at or above the surface throughout the year while dry dambos dry up. Most of the dambos are dry dambos that fill up during the wet season by rainfall and runoff from the surrounding woodlands. (Chidumayo, 1992).

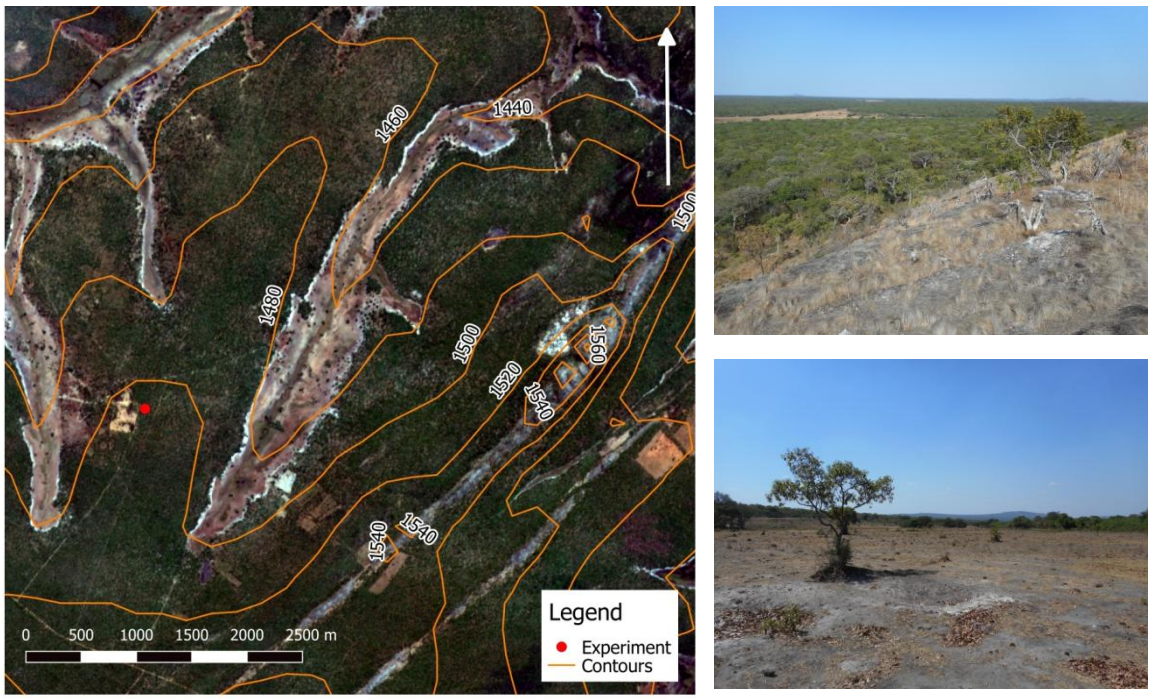

Figure 4 Elevation map of the surrounding area of the study site (left) and field images of the in-situ observations (right) made with data from Lehner et al. (2006) and a background of Sentinel images (Contains modified Copernicus Service information [2018])

The study site is located between several dry dambos which are covered by grass with an occasional tree. Due to the availability of grasses, the areas are often used for grazing game or livestock. The dambos are often burned in the dry season to get rid of moribund coarse vegetation that has been left after grazing in the wet season. The burning stimulates the re-growth of new and nutritious herbaceous and grasses. This has also been the case for the dambo areas surrounding the study site as is shown in the picture in Figure 4.

Tree species classification

The Miombo woodlands themselves are dominated by trees of the genera *Brachystegia* which are in some areas combined with trees of the genera *Julbernardia* and *Isoberlinia*. (White, 1983; Frost, 1996; Gumbo et al., 2018). There is, however, quite some tree species variation within the Miombo Woodlands due to differences in annual precipitation, soil characteristics and location. At the study site, an experimental area of 30 by 30 m is taken of which all the species are classified by their local names with tree knowledge of local workers. The translation of the local names to the scientific counterparts is shown in Appendix 3 and the results of the tree species count are shown in Table 1.

As the Miombo is quite heterogeneous, it is important to understand which type of trees are present in the study site especially due to the effect of the tree species on the transition period. The transition period is defined as the period in which the trees shed their leaves and experience a flush of new leaves. This flushing is also called green-up and depends on the tree species present. In addition, the trees have different phenologies that can be split into four categories (Table 1) which are evergreen, deciduous or a combination of the two which is either called semi-deciduous or semi-evergreen. The semi-deciduous trees are mostly deciduous but more than 25 percent is evergreen while for semi-evergreen trees, the trees are mostly evergreen but more than 25 percent is deciduous. (Land cover classification system, 2000) In the study plot most trees are (semi-) deciduous which agrees with the transition found in the Miombo.

Frequency (%)	Scientific name	Phenology
20	*Uapaca kirkiana*[1,3]	Semi-deciduous
13	*Brachystegia floribunda*[2]	Semi-evergreen
13	*Uapaca sansibarica*[1]	Semi-deciduous
9	*Bauhinia petersenia*[1]	Semi-deciduous
8	*Vitex doniana*[1,3]	Deciduous
7	*Julbernardia paniculata*[1,2]	Semi-evergreen
6	*Faurea saligna*[3]	Semi-deciduous
5	*Brachystegia longifolia*[1,2]	(Semi)deciduous
5	*Brachystegia spiciformis*[1,2]	(Semi)deciduous
3	*Pericopsis angolensis*[1,2]	(Semi)deciduous
2	*Anisophyllea boehmii*[4]	Semi-deciduous
2	*Swartzia madagascariensis*[1]	Deciduous
1	*Dischrostachys cinerea*[3]	Semi deciduous
1	*Garcinia buchananii*[1]	Evergreen
1	*Lannea discolour*[1]	Deciduous
1	*Maranthes floribunda*	Unknown
1	*Parinari curatelifolia*[1,3]	Evergreen
1	*Pterocarpus angolensis*[1,3]	Deciduous
1	*Unidentified*	NA

Table 1 Tree phenology of trees within the plot based on the reference according to their numbers: 1. Simmute et al. (1998), 2. Vinya et al. (2018), 3. Orwa et al. (2009) and 4. Nkengurutse et al. (2016)

The study site is located in an area with wet Miombo woodlands as defined by Chidumayo (1987) and White (1983). In White (1983), the wet Miombo wetlands are described as an area with over a 1000 mm rain a year and a canopy height of more than 15 m with dominant tree species such as the *Brachystegia floribunda, Brachystegia glaberrima, Brachystegia taxifolia*, *Brachystegia wangermeeana* and *Marquesia macroura*. In Table 1, it is shown that only the *Brachystegia floribunda* is indeed one of the dominant trees. The other dominant tree species mentioned by white are not found.

In Chidumayo (1987), the classification of the study plot is based not only on the precipitation but also on the trees species distribution. The study site is classified as northern wetter Miombo which is dominated by *Brachystegia spiciformis* and *Brachystegia utilis* with some *Julbernardia paniculata* and *Parinari curatellifolia*. Besides, the understory taxa consist of the

Monotes africanus, Syzygium guineense macrocarpum and *Uapaca species*. (Chidumayo, 1987). The species mentioned by Chidumayo (1987) are also found in the plot as shown in Table 1. One of the dominants *Brachystegia spiciformis* is found a few times. The *Brachystegia utilis*, however, is not found in the plot. Besides, the *Julbernardia paniculata* and the *Parinari curatellifolia* are both found as mentioned by Chidumayo (1987). Moreover, Chidumayo (1987) also mentioned a few of the understory taxa of which the *Uapaca species* are frequently found in the plot. As the *Uapaca species* are frequently found, the understory taxa can influence the outcome of this report.

As shown by the previous two examples from literature, some of the tree species are found while others are not. This can be due to the heterogeneity but also due to the frequent fires and the cutting of trees for resources such as timber, fruit, caterpillars, etc. Besides, there is a high amount of fruit trees such as *Uapaca kirkiana, Uapaca sansibarica, Julbernardia paniculata, Parinari curatellifolia* and *Pterocarpus angolensis* which could be due to their fruit-bearing capacity. (Richter and Cumming, 2005; Chidumayo and Frost, 1996)

Moreover, the area seems to be re-growth Miombo as the trees are often only about 10 m high. As shown by Chidumayo and Frost (1996) for dry Miombo the re-growth Miombo has a different composition of tree species than the uncut Miombo. It is, therefore, important to identify the state and the tree species present at the study site as Miombo woodlands as this can influence the data. In this case, the study site is located in re-growth Miombo which is influenced by human behaviour such as slash and burn cattle farming and used as a source of resources.

2.2 Methods to classify the green-up, shedding period and fire influences

The Miombo woodlands are known for their transition period in which the leaves are shed and reappear in what is called the green-up. The timing of this phenomenon differentiates each year as shown in Table 2. With a three month difference between the earliest and latest date within the wet Miombo, it is important to define the green-up period for the year 2018. The green-up period in Ryan et al. (2017) is defined as the period in which the trees will flush their new leaves before the start of the wet season.

Vegetation type	Mean day of year of green-up, G_{DOY}	Mean day of year of rain onset
Wet Miombo woodland	245 (205-297)	297 (262-327)

Table 2 The vegetation phenology and rainfall regime data (Ryan et al., 2017)

The satellite images will only register the total decrease or increase in vegetation seen from above, and as such will have difficulties differentiating between the green-up of the trees and the understory shrubs and grasses. According to Tian et al. (2018), there are different roles between the trees and the understory. Therefore, this report will distinguish two types of green-up periods, the first one is the green-up of the trees and the other is the green-up of the understory shrubs and grasses.

The period definitions will be based firstly on in-situ observations. These observations will serve as a first indication of the state of transition. The in-situ observations are, however, limited by the possibility to go into the field, and therefore, satellite images will be used to account for the periods in between. The visual bands of the Sentinel-2 images of 2018 (Copernicus Sentinel-2 data [2018]) will be studied to look for differences in vegetation. The periods are defined based on the first satellite images which shows a clear difference in appearance compared to the last one studied. The satellite images have a time step which is mostly not bigger than a week except during the rainy season. It will be assumed that the first time a satellite shows different images, the date is the start of the next period. Due to the weekly time step, the true date can differ a few days. The date used will, however, give a good indication.

Figure 5 Burning patches on the 21st of June (Copernicus Sentinel-2 data [2018])

Besides, the change in vegetation due to the phenology, vegetation is also heavily influenced by human behaviour. The Miombo Woodlands are altered through agricultural expansion, slash and burn, livestock rearing, settlements, gathering of wild foods and harvesting forest for timber and fuel. (Gumbo et al., 2018). One of the most impactful human practices at the study site is the burning of dambo and forest patches. This practice will be taken into account and given their periods. As an area of 30 by 30 m was fenced and therefore left undisturbed the natural transition without the influence of human-induced forest fires can be studied on a small scale. Satellites with a low resolution, however, suffer from the effects of forest fires.

In the results the locations of the forest fires are noted down. Similar to the transition period, the first time a dambo fire is noticed is taken as the start of the dambo fires until the last image that new fires are recognized. Fires are recognized by the black spots in the vegetation. A good example is shown in Figure 5, where the orange-reddish colour can be seen on the satellite image as well.

2.3 Methods to study vegetation indices

In this part, the methods of gathering and analyzing the vegetation indices such as the Normalized Difference Vegetation Index (NDVI), Normalized Difference Infrared Index (NDII) and Leaf Area Index (LAI) will be explained. The vegetation indices are based on the absorption of several components related to vegetation such as Chlorophyll, Mesophyll and water. In Figure 6, it is shown that healthy vegetation absorbs blue- and red light for the production of chlorophyll and starts the process of photosynthesis. While the NIR is reflected by the mesophyll which is where most chloroplasts are located and thus photosynthesis takes place. Besides, the SWIR region is sensitive to leaf water content due to the absorption of water molecules. (Ji et al.,2011 & National Aeronautics and Space Administration, 2010)

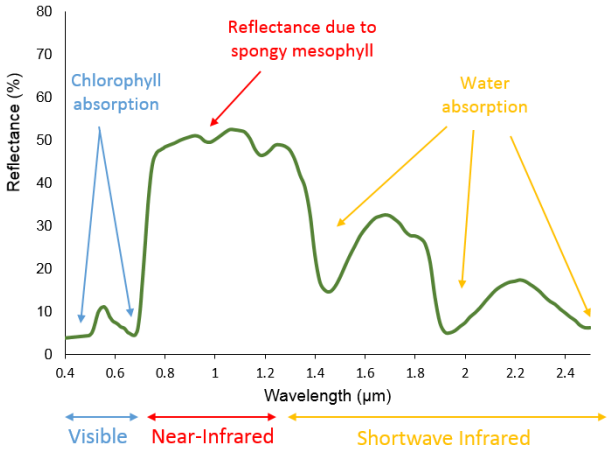

Figure 6 Absorption of vegetation related components (Vegetation and EMR, 2019)

A short description of the indices is given in the next sections. The three vegetation indices, however, have a lack of comparable points as the satellite images have a different time step and often do not match. Because of this, the correlation is made based on the average values for each month. This means that those monthly averages do not always have the same amount of points. This will also help with the analysis of the evaporation models as the indices are often used as inputs. By understanding the accuracy of the indices, the accuracy of the models can be understood better. Besides, the spatial resolution of the products is not always the same. In this case the MOD13Q1 250 m pixel will be taken as the area and the whole pixels of Landsat and Sentinel are averaged for the comparison.

2.3.1 Normalized Difference Vegetation Index (NDVI)

The Normalized Difference Vegetation Index (NDVI) correlates the photosynthesis and primary production of the vegetation (Wilson and Norman, 2018). The NDVI uses the difference in the reflection in the visible and near-infrared to determine the vegetation density. While the chlorophyll is absorbed with the red wavelength the mesophyll is reflected in the infrared segment. As they are both essential in the photosynthesis process, the healthy vegetation absorbs most of the incident visible light while it reflects a large portion of the near-infrared. In comparison, the unhealthy vegetation reflects more visible and less near-infrared. (Kinyanjui, 2010)

$$NDVI = \frac{NIR - Red}{NIR + Red}$$

In the process of photosynthesis, a combination of water and carbon dioxide is needed. This means that the amount of leaves is a good indicator for the parameters precipitation, evaporation and soil moisture (Szilagyi et al, 1998)

2.3.2 Normalized Difference Infrared Index (NDII)

The NDII can detect plant water stress as the leaf water content is negatively related to the SWIR as the leaves mostly absorb the SWIR. The NDII is strongly related to the moisture storage deficit in the root zone. (Sriwongsitanon, et al., 2016) The difference between the NDVI and the NDII is that the NDVI determines the vegetation density and the NDII is sensitive to the leaf water content. Besides, the NDVI is less accurate than the NDII in areas of grazing animals. (Wilson and Norman, 2018). In their research, the normalized difference infrared index (NDII) can track changes in areas with continued grazing better than the NDVI (Wilson and Norman, 2018). As the field plot is on a cattle farm where cows are continuously grazing, the NDII will also be taken into account.

$$NDII = \frac{NIR - SWIR}{NIR + SWIR}$$

2.3.3 Leaf Area index (LAI)

The Leaf Area Index (LAI) is defined as one half of the total green leaf area per unit horizontal ground surface area. As there are different definitions of the LAI, it is important to know if a product gives only the green leaves or also the non-green leaves. The first one is also called green LAI which is restricted to the green area which is active in photosynthesis and transpiration while the second one is the true LAI as it also includes non-green leaves.

Besides the different definitions, the satellite products also have different methods in which they calculate the leaf area index. For both the MODIS and PROBA-V outputs, the true LAI is given (Fang et al., 2019). The products, however, use different methods to derive the LAI. MODIS uses the Look-Up Table (LUT) while PROBA-V uses the Neural Network method. In addition to the LUT method, MODIS uses a back-up algorithm based on the relationship between the NDVI and canopy LAI to fill in data gaps.

MODIS – Look-Up Table (LUT)

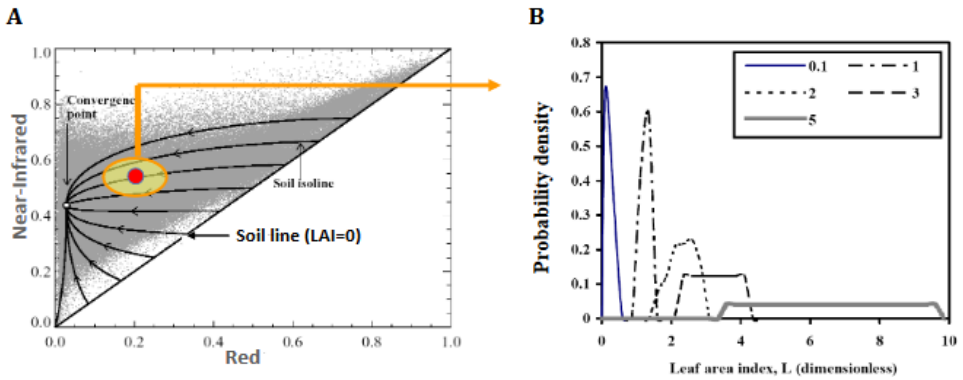

Figure 7 Illustration of the MODIS Look-Up Table method used to derive the leaf area index. Panel A: Distribution of vegetated pixels for the Red and NIR bands. An acceptable solution is each combination of the canopy/soil parameters and the corresponding FPAR values which is within the fellow ellipse. Panel B: Density distribution functions of the LAI for five different pixels. The mean LAI is taken as the LAI retrieval. (Knyazikhin et al., 1998, as cited in Knyazikhin et al, 1999)

In the Look-Up Table (Figure 7) the spectral information from the MODIS red and NIR surface reflectance bands is used to determine the leaf are index. The inputs are the vegetation structural type, sun-sensor geometry, bidirectional reflectance factors (BRF's) at the red and NIR spectral bands and uncertainties. MODIS tries to take into account three important features of the canopy radiation regimes:

1. The vegetation architecture
2. Optical properties such as leaves and stems
3. Physiological conditions such as water status and pigment concentration
4. Atmospheric conditions

The leaf area density distribution function (Panel B of Figure 7) is parameterized for specific intervals which are biome dependent. In the study site, the biome type is classified by MODIS as Biome 4: Savanna. Knyazikhin et al. (1999) describe the savanna biome as " *a canopy with two distinctive vertical layers, an understory of grasses, low ground cover of overstory trees, canopy optics and structure*". This means that the savannah is vertically heterogeneous which is also the case at the study site.

PROBA-V - Neural Network method

The PROBA-V uses a Neural Network method in which a machine learns to interpret the combined images. The Neural Network was trained with images of the SPOT/VEGETATION 1 km data to create the top of the atmosphere reflectance bands of the red, NIR and SWIR bands. As the bands of the SPOT/Vegetation are slightly different from the PROBA-V a spectral conversion is applied. Besides, the bands are corrected for atmospheric conditions. (Baret et al., 2013)

With the reflectance bands corrected, the Neural Network is trained to instantaneously retrieve the LAI, FAPAR, and FCover from the reflectance bands and geometry of acquisition. The training is done with true reflectance data and LAI estimates from a fusion of the existing products MODIS and CYCLOPES LAI. The fusing is done through a weighting which is designed to enhance the specific advantage of the MODIS and CYCLOPES products. Therefore, the PROBA-V product should be an enhanced version of these two. After training the neural network to provide the instantaneously LAI, FAPAR, and FCover products, the last step is to smoothen and fill the gaps based on the GLOBCOVER land cover map and the latitude. (Baret et al., 2013)

2.3.4 Vegetation indices products

The vegetation products used in this report are the MODIS, Sentinel-2, Landsat 8 and the PROBA-V products. The MODIS products have been extracted with the help of AppEEARS. For the NDVI, MODIS had several options, the raw data of MOD09A1 and the processed data of MOD13. As the MOD13 data also has been processed to remove outliers by averaging it over several days, this data set is chosen. For the NDII, however, MODIS does not have a pre-processed dataset and the data is retrieved by using the raw bands of the MOD09A1. For the LAI, MODIS again has a pre-processed data set and the MCD15A2H as this is only based on the Terra satellite similar to the other MODIS products.

For Sentinel-2 (produced from ESA remote sensing data [2018]), the data is gathered from the Copernicus Open Access Hub. After gathering the cloudless images, the data is brought into QGIS. Similarly, the Landsat 8 level-2 data is retrieved from the EarthExplorer USGS database (courtesy of the U.S. Geological Survey). Both the NDVI and NDII can be calculated by extracting the data points with the value tool of QGIS for the respective bands (Table 3). As the spatial resolution was not everywhere the same, the Landsat 8 and Sentinel-2 data have been adjusted for the spatial resolution of MODIS. All the pixels that were completely in the MODIS pixel, of Landsat 8 or Sentinel-2 have been averaged.

	Red	NIR	SWIR
Landsat 8 Oli/Tirs	4	5	6
MOD09A1	1	2	6
Sentinel-2	4	5	11

Table 3 Bands used for each satellite product

As MOD09A1 is the largest image, the Landsat 8 and Sentinel-2 are averaged over the area of MOD09A1 which is 500 by 500 m.

2.4 Description of the models used to study the effect of the transition period with the help of vegetation indices.

Evaporation cannot be directly calculated from remotely sensed data, and thus the evaporation has to be estimated indirectly. Models differ in both their indirect approach as in their definition of the evaporation. This report compares the outputs of three different types of models namely:

1. Surface Energy Balance System – **SEBS**
2. Global Land Evaporation Amsterdam Model - **GLEAM**
3. MODIS Terrestrial Evapotranspiration – **MOD16**

The three models differ on a theoretical basis and due to this different evaporation trends can be noticed as will be explained later on. First of all, SEBS is based on the surface energy balance and calculates the actual evaporation as a residue of the other parameters. GLEAM doesn't use the surface energy balance at all and MODIS only uses the radiation and soil heat flux to differentiate between the different evaporation fluxes.

While both GLEAM and MODIS calculate the evaporation through an equation based on the Penman-Monteith, the models have a completely different approach. GLEAM uses the simplified version of the Penman-Monteith also called Priestley-Taylor. The model is based on the potential evaporation and does not directly calculate the actual evaporation except for the interception flux. The stress factor is closely related to the soil water and thus precipitation seems to have a high impact on the evaporation values. MODIS, however, calculates the different evaporation fluxes one by one and then sums it all up to get the actual evaporation. The potential evaporation is a different formula which is still based on the Penman-Monteith.

Model	Spatial	Temporal
SEBS	0.05° latitude-longitude grid (± 5.5 by 5.5 km)	Daily
GLEAM	0.25° latitude-longitude grid (± 27.5 by 27.5 km)	Daily
MODIS (MOD16A2)	0.5 km	Every 8 days

Table 4 Spatial and Temporal Resolution of the evaporation model (Su, 2002; Martens et al., 2017 and Miralles et al., 2011b and Running et al., 2018)

The data from the models are extracted for the field work site, where the field experiments take place. The exact latitude and longitude coordinates are -12.378639 and 31.172079. These coordinates are used to extract the evaporation at the field work site. The evaporation models, however, have different temporal and spatial resolutions (Table 4). Therefore, the images have all been adjusted to the largest pixel of GLEAM by averaging the pixels of SEBS and MOD16A2.

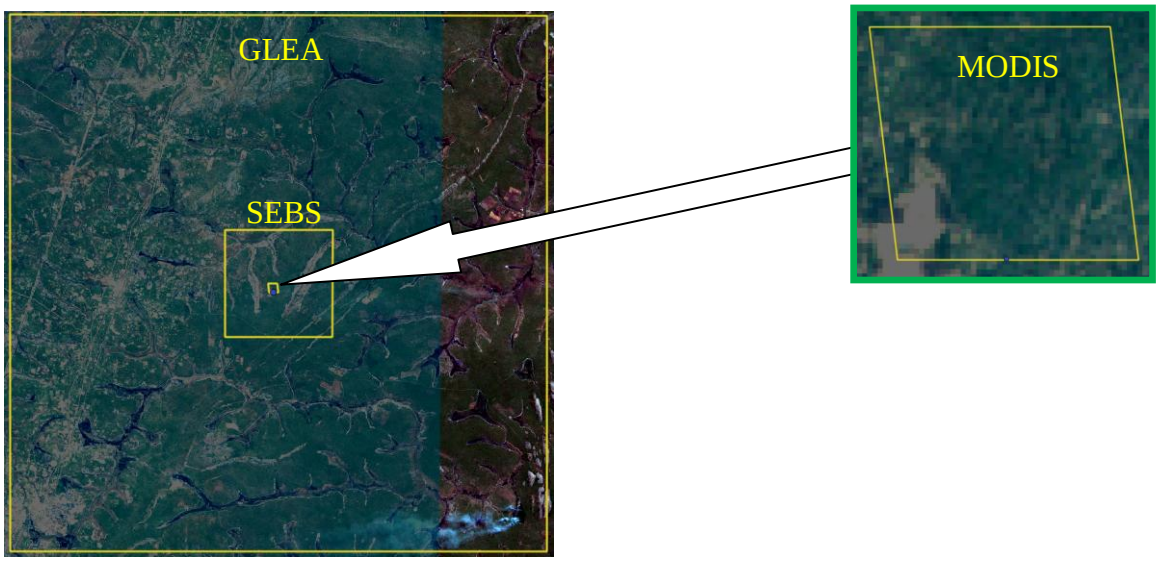

Figure 8 Spatial resolution of the models with a background of Sentinel images (Contains modified Copernicus Service information [2018])

2.4.1 Background on the Surface Energy Balance System – SEBS

SEBS uses a residual method of the surface energy balance to determine the evaporation. Besides, it is a single-source method which means that the net radiation (R_n), the soil heat flux (G_0) and the sensible heat flux (H) are based on the satellite information from the visible, near-infrared and thermal infrared bands in combination with meteorological data such as air temperature, wind speed, and humidity. (Li et al., 2009)

$$\lambda E = R_n - G_0 - H$$

The net radiation (R_n) is directly calculated with remotely sensed data while the soil heat flux (G_0) is taken as a ratio of the net radiation. The ratio is taken as an interpolated value based on the fractional canopy coverage (fc) between two limiting cases which are full vegetation canopy and bare soil. The other two parameters are derived through the boundary similarity theory. (Su, 2002) The Bulk Atmospheric Similarity theory is used in combination with a dynamic model for the thermal roughness to scale the Planetary Boundary Layer (PBL). In addition to this, the Monin-Obukhov Atmospheric Surface Layer (ASL) similarity is used for the surface layer scaling. (Li et al., 2009)

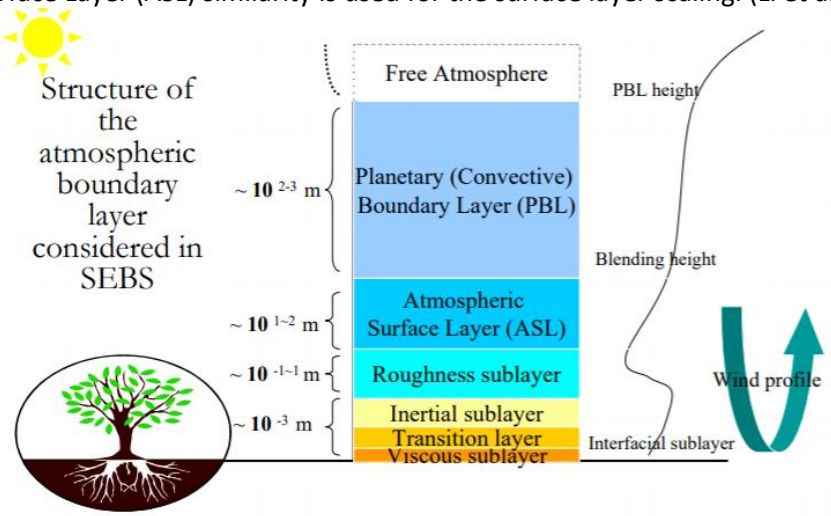

Figure 9 Atmospheric layers (Su, 2007)

The sensible and latent heat flux are derived with the help of these similarity theories as they describe the relationship between the surface and the atmospheric surface layer (ASL – Figure 9). In addition to this, SEBS has an extensive model for roughness for heat transfer to calculate the aerodynamic parameters required for the similarity theory. (Su et al, 2001; Su, 2002) Moreover, SEBS uses the contrast between the dry and wet limits to derive the evaporation and evaporative fraction for each pixel. (Li et al., 2009)

$$H_{wet} = \frac{(R_n - G_0) - \frac{\rho C_p}{r_{ew}} * \frac{e_s - e}{\gamma}}{1 + \frac{\Delta}{\gamma}}$$

Under dry condition the latent heat is assumed to be zero as soil moisture is limited and thus the sensible heat flux should be at its maximum level and thus $H_{dry} = R_n - G_0$. Under the wet conditions, the evaporation is assumed to be at its potential rate, λE_{wet}, and thus $H_{wet} = R_n - G_0 - \lambda E_{wet}$. The wet limit of sensible heat can be derived through the wet limit equation in combination with the Menenti equation which is based on the Penman-Monteith but also valid for non-vegetated areas. The actual evaporation is then calculated through the relative evaporation and evaporative fraction:

$$\Lambda = \frac{\lambda E}{R_n - G} = \frac{\Lambda_r * \lambda E_{wet}}{R_n - G} \; with \; \Lambda_r = 1 - \frac{H_{similarity\ theory} - H_{wet}}{H_{dry} - H_{wet}}$$

2.4.2 Background on the Global Land Evaporation Amsterdam Model - GLEAM

Similar to SEBS, GLEAM is also based on meteorological data and the remotely sensed data of the visual, near-infrared and thermal bands. Besides, GLEAM uses microwave data for the Vegetation Optical Depth (VOD) and soil moisture. These remote data sets are complemented with a static dataset describing soil properties, land cover and average rainfall climatology. (Martens et al.,2017)

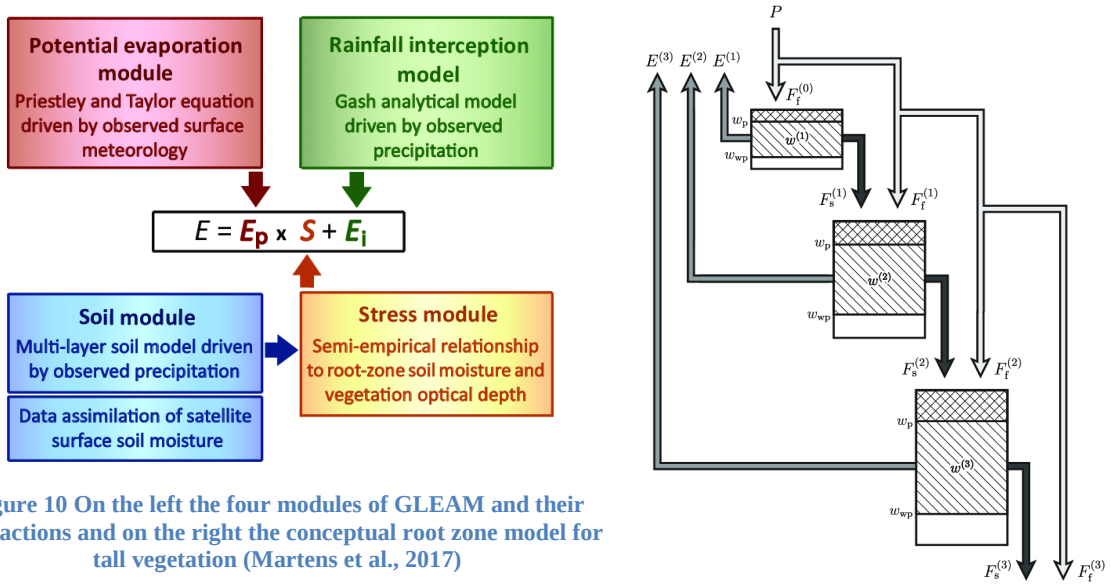

Figure 10 On the left the four modules of GLEAM and their interactions and on the right the conceptual root zone model for tall vegetation (Martens et al., 2017)

The actual evaporation of GLEAM is calculated with the help of four modules namely the potential evaporation module, the rainfall interception model and the soil module which forms the base for the stress module adjusted with a Newtonian Nudging Scheme to remove random forcing errors. The model firstly calculates the potential evaporation which is based on the Priestly and Taylor (1972) equation.

$$\lambda E_p = \alpha \frac{\Delta}{\Delta + \psi}(R_n - G) \tag{11}$$

For the actual evaporation, the potential evaporation is converted using a multiplicative stress factor (S in Equation XXX) which is based on the land cover type and depends on the soil water content, vegetation physiology and several phenological constraints (Martens et al., 2016). The stress factor decreases with a decrease in soil moisture as water becomes less readily available. (Martens et al., 2017).

$$\text{Short \& Tall vegetation:} \quad S = \sqrt{\frac{VOD}{VOD_{max}}}\left(1 - \left(\frac{\omega_c - \omega^{(\omega)}}{\omega_c - \omega_{wp}}\right)^2\right) \;\; \& \;\; \text{Bare Soil:} \quad S = 1 - \frac{\omega_c - \omega^{(l)}}{\omega_c - \omega_r} \tag{12}$$

The soil module forms the basis of the stress module and is a conceptual root zone model based on the water balance. The amount of soil layers that are taken into account for the root zone is dependent on the land cover. (Martens et al., 2016). The soil layers each exist of three different compartments (Figure 10):

1. First compartment: water that is unavailable for the root uptake as it is underneath the wilting point (ω_{wp}). For bare soil use the residual soil moisture (ω_r).

2. Second compartment: the maximum volume of water available for evaporation between the wilting point and the soil matrix.
3. Solid-phase of the soil column which cannot hold water.

The reduction of the potential evaporation provides a combined value for the soil evaporation and transpiration. The actual evaporation is produced after the interception is added. (Martens, et al., 2017). The interception module of GLEAM is based on the revised version of the Gash's analytical model by Valente et al. (1997). Interception is the part of the precipitation that is captured by the surface storage and evaporates before it can runoff or infiltrate into the soil (Gerrits, 2010). Therefore, the Gash's analytical model divides the rainfall into interception loss, free throughfall and stemflow. Besides, the model assumes that there is only one storm per rain day and that each storm has three phases which are the wetting phase, the saturated phase and the drying phase. (Valente et al., 1997)

2.4.3 Background on the Terrestrial Evapotranspiration MODIS - MOD16A2

The MOD16 algorithm calculates the evaporation as the sum of soil evaporation, interception, and transpiration. The algorithm is based on the Penman-Monteith equation and differentiates between day and night, wet and dry conditions and vegetation and bare soil surface. The latter is determined through the vegetation cover fraction, F_c. (Running et al., 2018)

$$\lambda E = \frac{s * A' + \rho C_p \frac{(e_{sat} - e)}{r_a}}{s + \gamma \left(1 + \frac{r_s}{r_a}\right)} = \frac{s * A' + \rho C_p \frac{VPD}{r_a}}{s + \gamma \left(1 + \frac{r_s}{r_a}\right)} \; with \; \gamma = \frac{C_p * P_a * M_a}{\lambda * M_w}$$

The net radiation (A') in the Penman-Monteith is calculated separately for canopy and soil surface. Besides, a distinction is made based on wet: $70\% \leq RH \leq 100\%$ and dry conditions: $RH < 70\%$ with $F_{wet} = RH^4$ and $F_{wet} = 0$ respectively. (Running et al., 2018) The total daily potential and actual evapotranspiration is the sum of the evaporation from the wet canopy, evaporation of dry canopy and the soil evaporation.

Actual evaporation: $\lambda E = \lambda E_{wet\,c} + \lambda E_{trans} + \lambda E_{soil}$

Potential evaporation: $\lambda E_{pot} = \lambda E_{wet\,c} + \lambda E_{pot\,trans} + \lambda E_{wet\,soil} + \lambda E_{soil\,pot}$

With the evaporation for wet canopy surface based on the Biome-BGC model (Thornton, 1998 as cited in Running et al., 2018).

$$\lambda E_{wet\,c} = \frac{\left(s * A_c + \rho * C_p * F_c \frac{e_{sat} - e}{rhrc}\right) F_{wet}}{s + \frac{P_a C_p \, rvc}{\lambda \, \varepsilon \, rhrc}}$$

The transition of the plants is dependent on the stomatal behaviour which is constraint by vapour pressure deficits (VPD) and temperature. The stomatal conductance is scaled to canopy level with the LAI and corrected with the variation in the atmosphere's temperature and pressure. This will then give the following formula for the actual and potential evaporation.

$$\lambda E_{trans} = \frac{\left(s * A_c + \rho * C_p * F_c \frac{e_{sat} - e}{r_a}\right)(1 - F_{wet})}{s + \gamma}$$

$$\lambda E_{pot\,trans} = \frac{\alpha * s * A_c (1 - F_{wet})}{s + \gamma} \; with \; \alpha = 0.26$$

The evaporation of the soil surface is divided into three different formulas. The first one is for the soil evaporation during wet conditions in which it rains and the soil is saturated. The second function is the potential soil evaporation after a rain event. And in the last case, the actual daily soil evaporation is calculated as a combination of evaporation during and after the rains. (Running et al., 2018)

$$\lambda E_{wet\ soil} = \frac{\left(s * A_{soil} + \rho * C_p(1 - F_c)\frac{VPD}{r_{as}}\right) F_{wet}}{s + \gamma \frac{r_{tot}}{r_{as}}}$$

$$\lambda E_{soil\ pot} = \frac{\left(s * A_{soil} + \rho * C_p(1 - F_c)\frac{VPD}{r_{as}}\right) (1 - F_{wet})}{s + \gamma \frac{r_{tot}}{r_{as}}}$$

$$\lambda E_{soil} = \lambda E_{wet\ soil} + \lambda E_{soil_{pot}} \left(\frac{RH}{100}\right)^{\frac{VPD}{\beta}} \quad with\ \beta = 250$$

3. The five vegetation periods and the influence of human-induced fires in 2018

In Figure 11, four pictures of the Miombo forest during four different field trips during the transition period are shown. The transition period is defined as the total period in which the trees shed their leaves to the reappearance of tree leaves. The transition period starts with the shedding of the tree leaves. The reappearance of fresh new leaves can also be called green-up. (Ryan et al., 2017) The images in Figure 11, show a clear distinction between the response of the trees in the dry season and the grasses. While in August most of the grasses were already gone, the trees were still fully leaved. It is likely, that the grasses will wither early on due to the shallow rooting depth while the trees will be able to reach the deeper groundwater reservoir and thus shed their leaves at a later moment. That is why there will also be two shedding periods defined. One for the withering of the grasses and one for the shedding of the leaves.

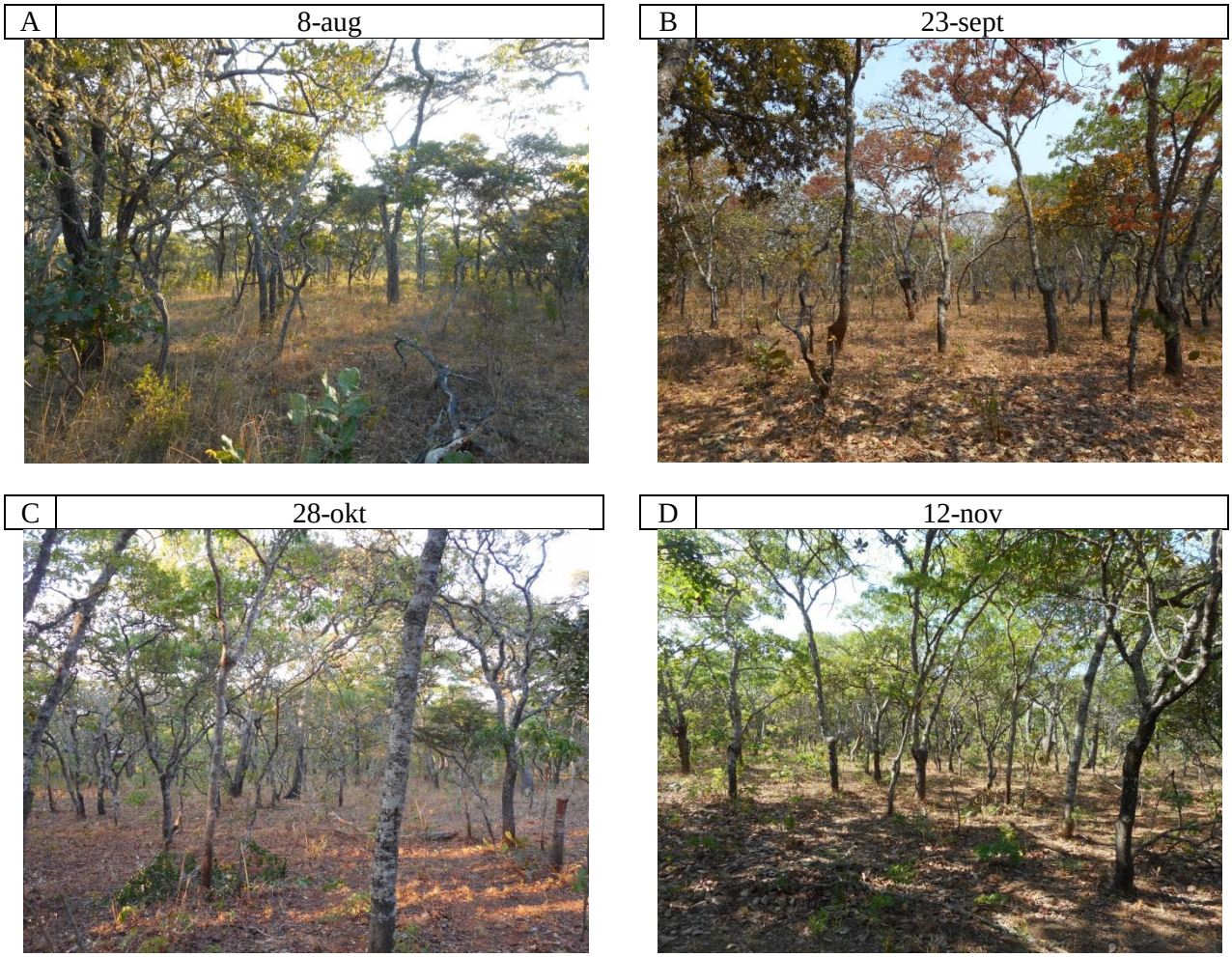

Figure 11 Transition on the ground, pictures on and around the study site from the four field trips

Figure 11A, which is taken on the 8th of August, shows the forest after the withering grasses. It represents the period in which the trees are still fully leaved and green but most of the understory is already gone. The understory grasses have a yellowish colour which indicates a lack of water in the shallow part of the soil. In Figure 11B taken on the 23rd of September, the forest has transformed. The trees have started to shed their leaves and different shades of leaves re-appear. A dominant feature is the appearance of red leaves which is due to a high amount of anthocyanins that occur in young leaves of the Brachystegia genera (Chidumayo and Frost, 1996).

At the end of September, it is clear that the trees are in transition. As shown in Figure 11C, the red leaves disappear in the next month, as there are no red leaves on the 28th of October. The image shows a forest in which new leaves are still re-appearing. Besides, a new green understory has not yet reappeared. The transition of the trees, however, is not yet over as the trees are much greener at the beginning of November than at the end of October. (Figure 11D)

The forest is probably a lot greener in November than in October since the timing of the flushing of green leaves depends on the tree species. This is clearly shown in Figure 12, where four different trees are shown on a 360° picture while the trees on the right are already fully leaved, the trees on the left are still getting new leaves. This is also confirmed by Vinya et al. (2018). In this article, nine tree species, which are common in the Miombo woodlands, were compared based on their stem water potential. According to the data found by Vinya et al. (2018), the different tree species have different stem water potential values which are triggering leaf shedding and flushing. In this article, the shedding of leaves was often from July to September and the flushing often started from September to October. This will be taken into account later on.

Figure 12 Fish-eye lens picture of four different tree species on the 4th of October.

On the last field trip on the 12th of December, the rains had started which brought a flush of new green grasses. Due to rainfall distortion of the forest image, the image is not included in Figure 11. Figure 13, however, should indicate the green-up in the forest as it shows the flush of new green grasses at the farm site. Besides, the picture shows the bare soil which was seen from the first to the fourth field trip.

Figure 13 Bare soil in the first field trip (picture of the 5th of August) and the newly grown grasses at the last field trip (picture of the 12th of December)

These field observations can only give indicate possible periods due to their temporal limitations. Besides, the literature is based on a different patch of forest and some of the trees species vary due to the heterogeneity of the forest. Because of these limitations, the satellite images of the visual spectrum of the Sentinel-2 imagery are studied to fill in the gaps between the fieldwork and get results of this patch of forest. The results are shown in Figure 15.

The figure distinguishes four vegetation stages and three types of fire periods. The first phenology stages characterize itself with a high amount of vegetation and a green dambo as shown in image 1 and also still in image 2 although it is less green. This stage represents the period in which the vegetation has access to water due to rains. As most of the water comes from the rains the period is similar to the period of the rainy season. This stage is from the beginning of December to the beginning of May as shown in the pictures.

The second stage is the stage where the grasses start to wither and disappear; this is according to the Sentinel visual spectrum images from the beginning of May to the beginning of August. This is the stage in which the dambo slowly lose their green colour which is shown in the comparison of image two and three. You see that the values in Appendix 1 start to increase from the beginning of August on, for both the Blue as the Red band but not for the green band. As the reflection of the Red band increases, it is highly likely that this is the shedding period.

Then at the end of August, the values of the green band start to increase as well although the values are fluctuating. (Appendix 1) This is probably because some species are still shedding while others are flushing leaves. This is also confirmed by Vinya et al. (2018) as different tree species have different shedding and flushing seasons. Therefore, the forest is never completely bare but trees are in different stages of transition throughout the transition period. This will still be defined as a shedding period though due to the fluctuations.

From the 10th of October on, the vegetation keeps increasing while the red visible band is decreasing. (Appendix 1). This is in line with the new reddish leaves of the Brachystegia spotted on the 23rd of September as they have disappeared during this time. Because of this the 10th op October is defined as the start of the Green-up at the field site in 2018. According to the field observation there is still no grass on the 12th of November but it will appear on the 12th of December. This is in line with the decrease in the red band. Therefore the Green season starts on the 8th of December.

Period	Start date	End date
Green season	13th of December	11th of May
Withering grass season	12th of May	9th of August
Trees shedding season	10th of August	9th of October
Green-up period trees	10th of October	12th of December

Table 5 Period definitions used throughout the report based on observation results from in-situ observations and satellite imagery.

The last stage of the phenology is the green-up from the forest floor which happens from mid-December and into the next year. This is the start of the Green season again. As the dambos are burned, the grasses have not yet grown in December. At the farm site, however, slowly seem to disappear as it becomes greener (Image 5 and 6 of Figure 15). This is similar to what was found in the in-situ observations. The overview of the phenology stages is shown in Table 6.

Period	Start date	End date
No fires period 1	12th of December	15th of June
Early dambo fires	16th of June	21st of June
No fires period 2	22nd of June	18th of September
Forest fires	19th of September	23rd of October
Late dambo fires	24th of October	11th of December

Table 6 Period definitions used throughout the report based on observation results from in-situ observations and satellite imagery.

As the phenology is influenced by the forest fires, the satellite images are used to define a period in which the fires occur. The first fires start already at the beginning of June. These fires characterize themselves by the fact that they happen mostly in the dambo areas. The first forest fires have only been spotted from the beginning of September. September and October are also the months in which most forest fires occur. In Figure 14, the dates of the forest fires and the areas of forest fires are shown. As the forest fires of the 19th and 24th of September are quite extensive, this should be seen by the vegetation indices and thus also evaporation products. At the end of October, no more forest fires are found and the last fires are again mostly in the dambo areas. As the fires in the dambo areas are quite late in the dry season, the fires are likely responsible for the dambo areas being bare in December.

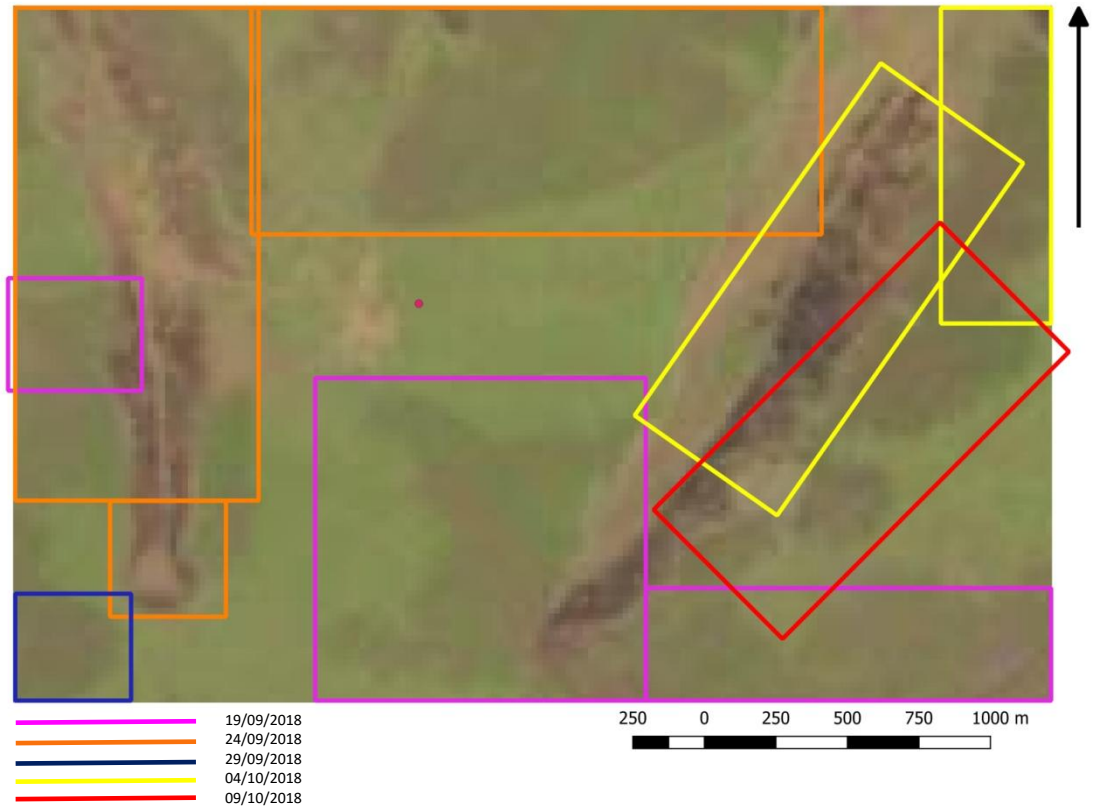

Figure 14 The dates and areas of the forest fires with a background of Sentinel-2 Visual bands image (Contains modified Copernicus Sentinel data [2018])

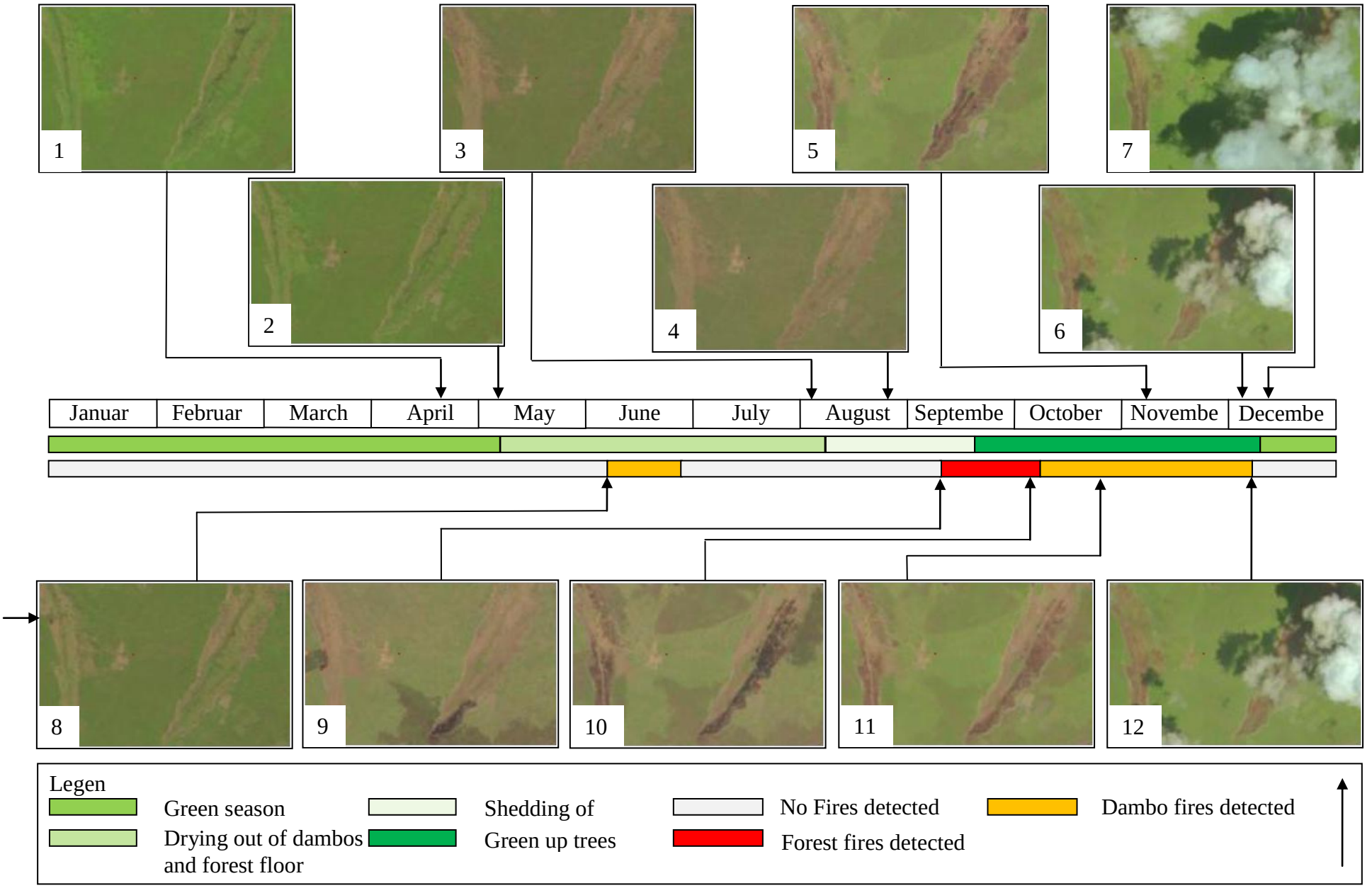

Figure 15 Changes in the Sentinel-2 Visual Spectrum related to the phenology and dambo and forest fires (Contains modified Copernicus Sentinel data [2018])

4. The effects of the transition period on the evaporation

In this chapter, the evaporation models are compared to each other and the previously defined vegetation stages. The first thing to notice is the completely different evaporation trends between the end of July and November which is also the period in which the transition period takes place. The first striking feature is the direct evaporation response from the GLEAM model after rainfall events. This is likely because the soil module is a conceptual root zone model based on the water balance. This model determines the stress module which is decreasing the potential evaporation. As the fluctuations in the green season are quite big and the evaporation seems to go down to almost zero before the first rains in November, the water stress seems to be overestimated.

This is especially clear in the months September and October in which the trees flush their leaves but GLEAM still goes down in Evaporation. With the first rains in November, the evaporation according to GLEAM shoots up quite rapidly which is unrealistic as the vegetation doesn't change much in November according to the field observations. There are several reasons for the overestimation of the stress module in GLEAM. First of all, the soil module only goes up to a depth of 250 cm. Therefore, GLEAM only takes into account up to 250 cm of the root zone while Miombo trees can root deeper than 250 cm as a taproot of some of the Brachystegia and Julbernardia genera can exceed 5 m in deep soils. The model can be adjusted for a deeper root zone and can probably better estimate the evaporation.

Besides, the model assumes that the available groundwater can be estimated through a simple drainage algorithm. This means that the model does not take into account any horizontal or upward fluxes. The soil module is thus fully based on the net precipitation and does not take into account any of the groundwater fluxes that are not related to the precipitation.

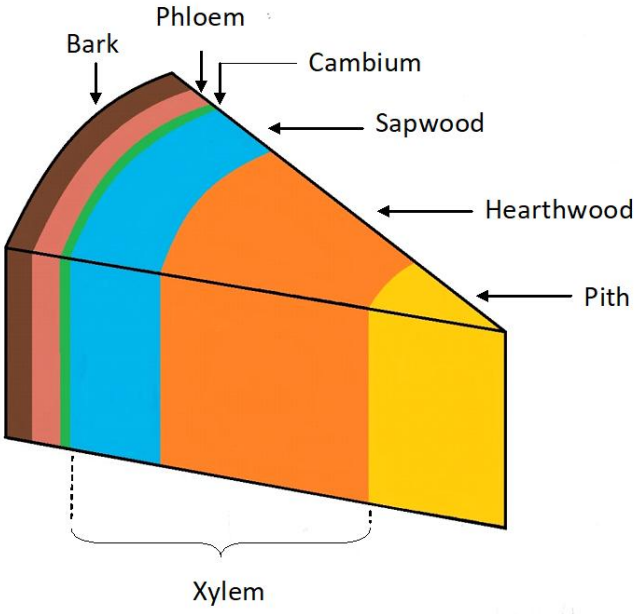

Figure 16 Explanation of different tree areas

Another possibility, according to Higgins et al. (2011) is that the early-flushing strategy is similar to the stem succulent strategy by Borchert & Rivera (2001) except for the synchronous leaf abscission. According to Borchert and Rivera (2001), tropical stem-succulent trees can store large quantities of water in their stems. Due to this, the trees can sprout weeks before the first rainfalls of the wet season. This is also confirmed by Vinya et al. (2018) as they studied the changes in plant water relations. In the study of Vinya et al. (2018), the seasonal minimum stem water potential was reached when the leaves are shed. Besides, the xylem (Figure 19) rehydration happened directly after the flushing of new leaves which suggests that the Miombo trees store water in their stems.

The storage of the water in the tree stems is also confirmed by Tian et al. (2018), as the Miombo trees grow the cambium area (Figure 19) by making new vessels during a short period late in the rainy season. This means that the Miombo makes use of an endogenous whole-plant control of leaf phenology (Tian et al., 2018) and the water stress is less high than GLEAM suggests.

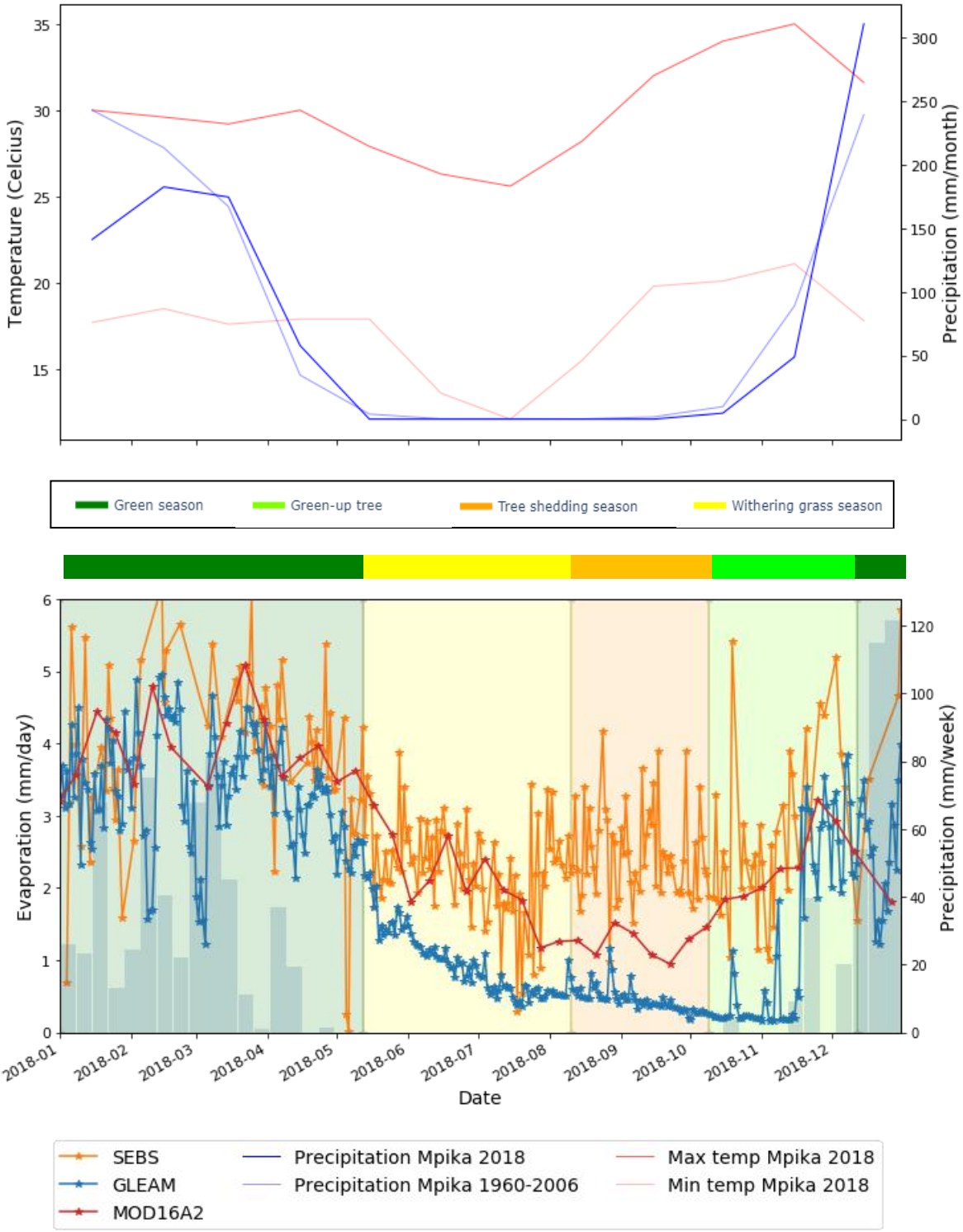

Figure 17 Comparison of the Evaporation Models in each of the defined seasons and the temperature and precipitation trend throughout the year 2018. (Mpika Weather Station, 2019; Su, 20002; Marten et al., 2017 & Miralles et al., 2011b and Mu et al., 2013)

While GLEAM didn't react to the transition period, SEBS and MODIS both react in different ways. Similar to GLEAM, SEBS decreases after the peak in mid-March. SEBS differs, however, from both GLEAM and MODIS due to its rapid increase in mid-July and the decrease in October before a rapid jump in November. As the transition period has not yet started, another explanation has to be found. One of the reasons for the rapid changes could be the start of the slash and burn. As SEBS is based mostly on temperature and radiation, the slash and burn practice could have a higher impact on the evaporation output of SEBS than of MODIS and GLEAM. Another explanation could be the increase in temperature which is around the same time as the rapid increase in mid-July influence the other parameters. Li et al. (2009).

Especially as the surface temperature is an important parameter to establish the link between the surface radiances and the surface energy balance components. The surface temperature is not only needed to calculate the net radiation but also the soil heat flux as this flux is based on the ratio of soil heat flux to net radiation. Besides, the sensible heat flux is sensitive to changes in temperature as it is based on the wind speed, the temperature at the reference height and the surface temperature. (Su, 2002) This means that all the different components of the energy surface balance are partly based on the surface temperature. Moreover, the Surface Energy Balance System calculates the evaporation as a residue of the other three components which means that the evaporation is extremely sensitive to temperature changes as it influences all three components it is based on.

As the surface temperature increases around mid-July, it is only logical that the Surface Energy Balance System reacts. Besides, to the natural temperature increase the slash and burn practice can also further drive up the temperature. Also, the days become longer again as the shortest day has been on the 21st of June. This means that more solar radiation will reach the Earth's surface. The combination of increasing temperature, incoming solar radiation and the slash and burn practice probably lead to a rapid jump in the model as the transition period has not yet started. Therefore, it is unlikely that the increase is due to the transition period.

After the rapid increase in the evaporation values, SEBS fluctuates around the same values until about mid-October in which SEBS decreases again to increase with the start of the rainy season. May SEBS react this way because SEBS is based on the contrast between dry and wet limits. SEBS assumes that there is no evaporation under the dry-limit. As explained before, the Miombo trees can store large quantities of water in their stems and therefore, the dry-limit may not be as dry as assumed. This would also explain why SEBS can react well throughout the year except for mid-July to October which is the driest period of the year.

All in all, SEBS reacts in some way to the transition period. The response, however, does not follow the vegetation stages. SEBS increase while the trees are shedding their leaves. In the shedding season, SEBS seems to stay around the same value while the field observations and the vegetation indices in the previous chapter shows a clear decrease in this period. At the end of October, SEBS evaporation values suddenly drop while this is the green-up period. SEBS is thus contradicting the behaviour of the vegetation.

MODIS also decreases from mid-March but does so until the beginning of August. This is in line with the withering of the grasses. During the tree shedding season, however, MODIS does not change much even though the vegetation indices from the previous chapter show a decrease in vegetation. MODIS even shows a small increase at the beginning of September. This could be due to the young reddish colour leaves of the Brachystegia. That the evaporation value during the shedding season stays mostly the same could be because of different species time the shedding of the leaves and the flushing of new green leaves differently. Because of this, some species are shedding while others are flushing new leaves. Therefore, it could be that MODIS is accurate in this month and the evaporation does indeed not change. Further research is needed to answer this hypothesis.

At the end of September, MODIS starts to increase again. This is a bit earlier than the defined green-up. As the vegetation indices also were a bit earlier than the defined green-up, it could be that the green-up is at the end of September instead of the beginning of October and therefore MODIS

could again be accurate. Nevertheless, MODIS starts to fluctuate with the start of the first rains and is no longer accurate after this first rain event. For the transition period, however, MODIS is the most accurate in its timing to the changes in vegetation.

The higher accuracy is probably because MODIS has an extensive model in which the interception, transpiration and soil evaporation are calculated separately. The Net radiation is calculated in a similar way to SEBS but that is also where most of the similarities end. As SEBS calculates the evaporation as the residue of the energy surface balance and MODIS calculates the evaporation as the sum of all the different types of evaporation. The disadvantage of MODIS, however, is that the model requires a lot of parameters.

Evaporation as input for your model

Evaporation (mm/day)	SEBS	GLEAM	MODIS
2018	1045	686	970
Percentage of SEBS	100%	66%	93%
Percentage of GLEAM	152%	100%	141%
Percentage of MOD16A2	108%	71%	100%

Table 7 Annual evaporation comparison

As explained above, the three models have different trends especially during the shedding and flushing of new leaves. So, what is the influence of these differences if you use the different evaporation models as input for your model. As shown in Table 7, the annual evaporation values are quite different. SEBS gives you 50% more evaporation per annual than the GLEAM output. The SEBS and MODIS output are however quite close to each other with less than 10% difference on an annual basis. If only the shedding and flushing period of the trees is taken into account, the differences increase with especially low values for GLEAM as SEBS is three times and MODIS two times as much. Also the difference between SEBS and MODIS is substantially bigger.

Evaporation (mm/day)	SEBS	GLEAM	MODIS
10/08/2018-13/12/2018	320	110	226
Percentage of SEBS	100%	34%	71%
Percentage of GLEAM	291%	100%	205%
Percentage of MOD16A2	142%	49%	100%

Table 8 Shedding/flushing period evaporation comparison

While the annual and shedding/flushing amount values of GLEAM are off compared to the other two models, SEBS is the one with the lowest correlation. With values between 59 and 70 percent. (Appendix 5). This while GLEAM correlates well with MODIS except during the shedding/flushing period as shown in Figure 20. The low correlation of SEBS has probably to do with the fluctuations in the transition as these fluctuations happen during the slash and burn practice, it could be that SEBS is correctly measuring the values but gets noise from the smoke of the slash and burn practice.

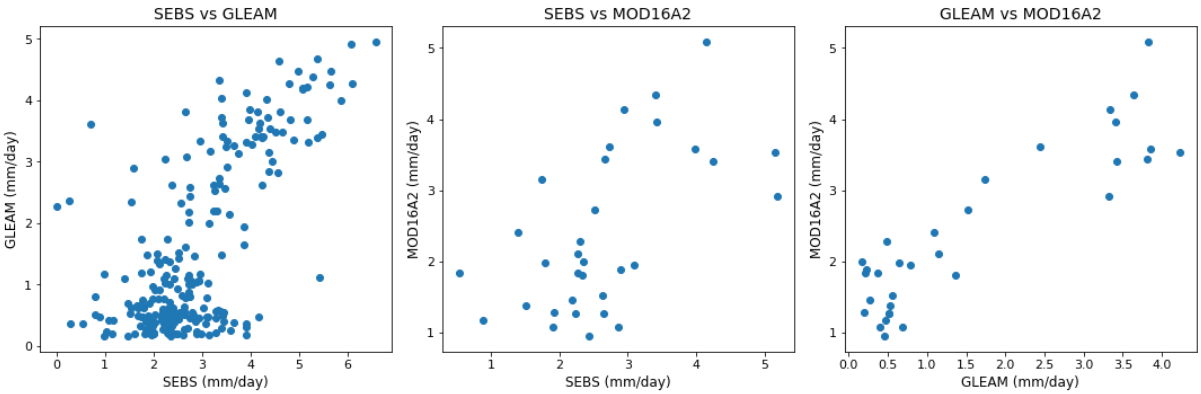

Figure 18 Correlation of the evaporation models

5. The effects of the transition period on the vegetation cover

In this chapter, the vegetation stages, as defined in chapter 1, are compared to the Normalized Difference Vegetation Index (NDVI), Normalized Difference Infrared Index (NDII) and the Leaf area index (LAI). For the NDVI, the MOD13Q1 is chosen due to its lowest spatial resolution of 250 m, the MOD13A1 and MOD09A1 output can be seen in Appendix 2 together with the NOAA-19 AVH13C1 output. The NOAA-19 data is left out of the comparison due to its oscillations. The results of the three NDVI, NDII and LAI outputs are shown in Figure 19. The satellite products of MODIS, Landsat 8, Sentinel-2 and PROBA-V produce similar trends for the vegetation indices with slight differences in the timing of certain peaks and troughs.

The indices show their highest values during the wet season. The NDVI and NDII have their highest vegetation values around March while the PROBA-V shows a peak from December to January. The rainfall is highest in December for the rainy season of 2017-2018 (Mpika weather station, 2019). It is, therefore, likely that the highest vegetation peaks are shown afterwards due to the abundance of water available. As the precipitation amount decreases at the end of March, the indices show their first decrease in vegetation. The products of the vegetation indices start to decrease around mid-March.

The green season is currently defined until the 11th of May, it is however likely that the green season is a bit shorter and already ends in April as the vegetation indices are already decreasing for a little while. Besides, the PROBA-V LAI starts to decrease more rapidly from mid-April. The images of the dambos of Sentinel show, however, that the dambos are still green in May. This could be because it is located lower than the forest. At the same time, the farm area to the left of the experiment is already quite bare. This, however, could also be influenced by the grazing cattle. Nevertheless, the dambos are lower laying areas (Figure 4 in Methodology), and therefore, the area could be wetter than the surrounding forest areas. It is thus likely that the green season ends at the end of April instead of the beginning of May. With the last rainfall being on the 27th of April, this could be redefined as the end of the green season.

After the green season, the grasses start to wither and the trees start to shed their leaves. The trees, however, shed their leaves quite late into the dry season. According to Chidumayo and Frost (1996), the leaf fall happens mostly from August to October. This is also the period in which the NDVI strongly decreases and hits its lowest point. The NDII is, however, a bit earlier with a strong decrease starting at the end of July. The lowest point is already hit in August and continues until mid-October. The NDII values get below zero at the end of July to the beginning of August depending on the satellite product.

As the NDII indicates water stress (Sriwongsitanon et al., 2016), the negative values could mean water stress. As the patch of forest wasn't burned since it was fenced, the most likely explanation would be the leaf abscission. This would also work, the other way around if the end of the green-up date is taken into account. This would be when the NDII reaches above the zero line again. This is around mid-October which is also when in the field observations most of the forest is already starting to become greener. The trees are, however, still becoming much greener until November and some trees may even do so until mid-December. Therefore, the zero line is not an indication of the grass and tree distinction, the zero line could indicate the largest part of the transition period but not the total contribution of the trees to the NDVI, NDII and LAI indexes.

As the first grasses were observed during the fieldwork at the beginning of December, it would be more likely that the increase in NDII and also NDVI at the end of October to the beginning of November is due to the green-up of the trees than the grasses. This would also be in line with the grasses' quick response to rainfall as argued by Chidumayo (2001). In Chidumayo (2001), the difference between leaf phenology of woody or tree and herbaceous or grass components is explained. While the trees already start shooting one to three months before the start of the rainy seasons, grasses are often restricted by the rainy season.

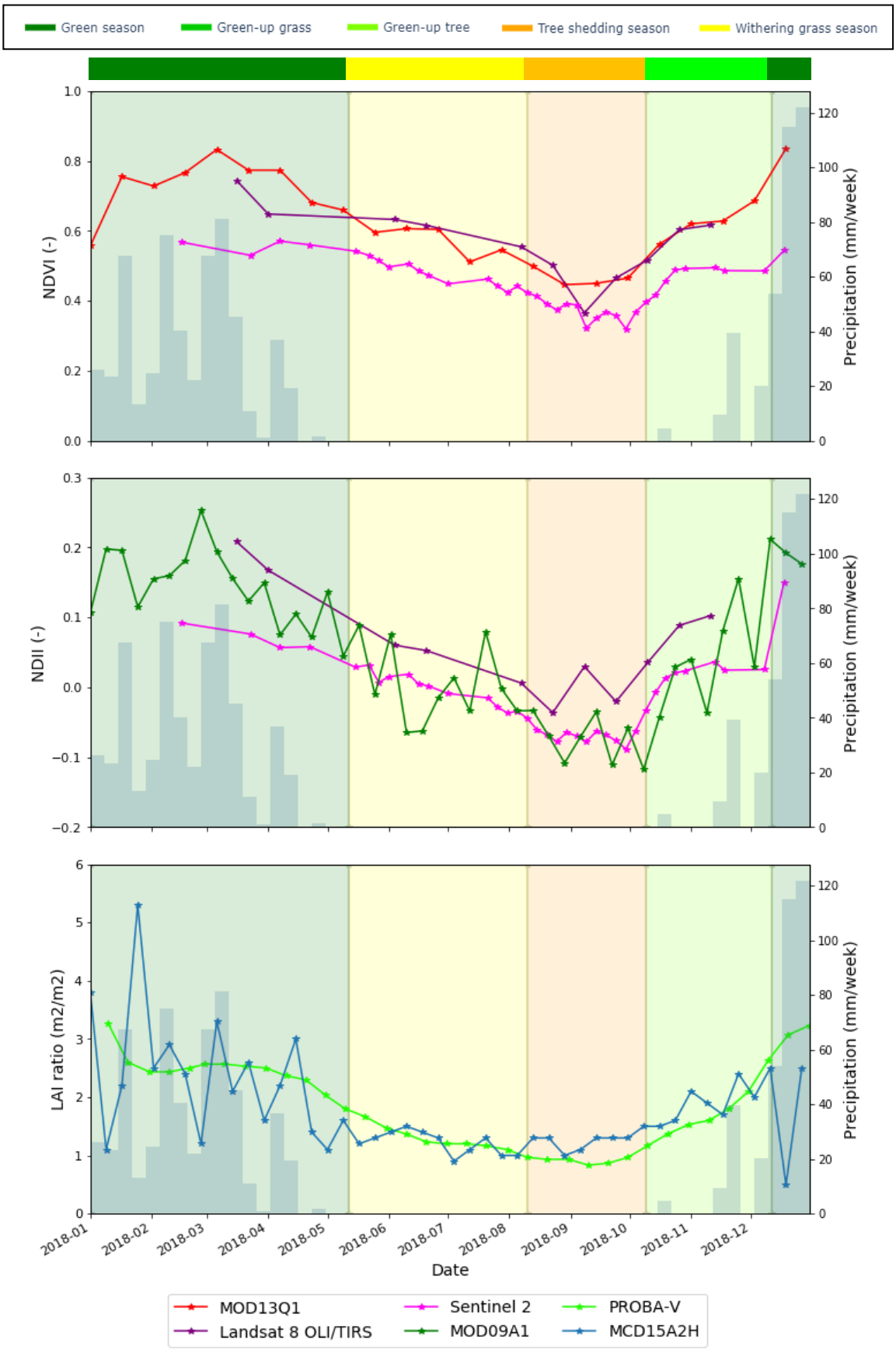

Figure 19 Trend lines of the NDVI, NDII, and LAI in 2018 (Didan, 2015; Myeni and Knyazikhin, 2015; Vermote, 2015; Contains modified information from Landsat-8 images courtesy of the U.S. Geological Survey and Copernicus Service information [2018])

Chidumayo (2001) simplifies the split between the increase in NDVI due to trees and due to grasses. The increase in NDVI in August/September to December is taken as an indication of tree leaf growth and the growth in January to March as grass growth, the withering of grasses should thus be until the end of May. Afterwards, the trees will lose their leaves until the lowest points are reached around September. This would mean that the withering grass season is overestimated and the effect of the shedding is underestimated in the current period definition. It is, however, hard to estimate the exact contribution of the grasses and leaves to the vegetation indices as the periods of withering and growth can overlap.

The results of both the field observations in the previous chapter and the NDVI, NDII and LAI output suggest that the simplification used in Chidumayo (2001) is oversimplified for December as grasses have already sprouted and the indices are close to their maximum values. Therefore, the end of the wilting grass season will be kept as defined in Chapter 1. Especially as the rapid decrease of the NDVI and NDII in August and September suggests that the trees mainly shed their leaves around this period. In contrast to the rapid decrease in NDVI and NDII, the LAI does not seem to change much during August and September. It is likely because the LAI takes not only green but also reddish leaves into account. This is important as the main tree species are of the Brachystegia genera and those trees flush their young leaves with a reddish colour which is created by the anthocyanins. (Chidumayo and Frost, 1996).

After the wilting of the grasses, the trees start to shed and the shedding season starts. As mentioned before, according to Chidumayo (2001), this is around August and September and thus in agreement with the previous chapter defined start in August. Besides, the length of the shedding season defined in the previous chapter seems to also be quite alright when compared to the vegetation indices outputs. For the NDVI, the MOD13Q1 and Sentinel-2 seem to agree with the end of the leaf fall and start of the green-up around the end of September to the beginning of October. Landsat, however, already increases at the beginning of September. This seems to be a bit early as field observations showed that while new leaves were reappearing in the form of sprouts, many trees were still shedding their leaves.

This field observation shows that the shedding and flushing of new leaves happen around the same time. This is because the shedding and flushing are tree species-dependent. Therefore, if the shedding period is mentioned, this means that the shedding of leaves is dominant regarding the flushing of new leavers. This also shows us the main problem in regards to the satellite outputs, as the Miombo woodlands are very heterogeneous. This is also why different plots of Miombo woodlands are difficult to compare. The indices can, however, give an overview of the dominant mechanisms in a certain moment. This heterogeneity could also be the reason for the two peaks and troughs of Sentinel-2 in the NDVI data. Other possibilities are the influence of the smoke forming as the areas surrounding the plot are affected by slash and burn practices. In this case, the previously defined areas which are based on combinations of field observation and the visual spectrum images of Sentinel-2, give a good indication of the trends shown in the vegetation indices. The only thing that is changed is the border between the green season and the withering grass season.

Influence of vegetation indices on evaporation models

The vegetation indices are inputs for the several evaporation models. As shown in Appendix 5, the different vegetation indices sources barely differ from each other. The indices themselves, however, are slightly different. In this part, the vegetation indices are compared and it is discussed if these input variables are the reasons for the different outputs of the evaporation models. SEBS uses mostly the Leaf Area Index (LAI), but can in case of no LAI data use the Normalized Difference Vegetation Index (NDVI) data as well. MOD16A2 only uses the Leaf Area Index (LAI). GLEAM on the other hand uses neither NDVI and LAI. Another index to calculate the vegetation changes is the Normalized Difference Infrared Index (NDII), this index is compared with the NDVI and LAI to see if this index responds differently.

2018	SEBS		SEBS	
	Pearson	p-value	Pearson	p-value
NDVI *MOD13Q1 *Sentinel	**0.689**	1.1E-3	0.508	2.6E-3
NDII * MOD09A1 * Sentinel	0.380	0.035	0.535	1.6E-3
LAI *MCD15A2H *PROBA-V	0.450	0.011	**0.657**	9.0E-4

Table 9 Pearson correlation between SEBS and vegetation indices
*Zero points between SEBS and Landsat

In Table 9, the Pearson correlation between SEBS and the vegetation indices is shown and it shows a small correlation between the MOD13Q1 NDVI and the PROBA-V LAI and SEBS. The model, however, seems only partly forced by the vegetation indices which makes logical as the model is based mostly on atmospheric parameters such as radiation and temperature.

2018	GLEAM		GLEAM		GLEAM	
	Pearson	p-value	Pearson	p-value	Pearson	p-value
NDVI * MOD13Q1 * Landsat * Sentinel	**0.796**	**5.6E-6**	**0.686**	**0.020**	**0.746**	**7.7E-8**
NDII * MOD09A1 * Landsat * Sentinel	**0.756**	**2.7E-9**	**0.796**	**3.4E-3**	**0.709**	**6.2E-7**
LAI *MCD15A2H *PROBA-V	0.489	**5.6E-4**	**0.783**	**1.7E-8**	**X**	**X**

Table 10 correlation between GLEAM and vegetation indices

In Table 10, all the vegetation indices except the MCD15A2H seems to correlate about 70% or higher. The GLEAM evaporation is thus strongly related to the vegetation indices even though none of them are used as an input. Gleam uses soil moisture as an input which could be responsible for the correlation as it is directly linked to the water available for the vegetation.

2018	MODIS		MODIS	
	Pearson	p-value	Pearson	p-value
NDVI * MOD13Q1 * Sentinel	**0.853**	4.460	**0.942**	0.058
NDII * MOD09A1 * Sentinel	0.738	1.6E-8	**0.963**	0.037
LAI *MCD15A2H *PROBA-V	0.572	6.1E-5	**0.999**	1.5E-3

Table 11 correlation between MOD16A2 and vegetation indices
*Zero points between SEBS and Landsat

Interestingly, the NDVI, NDII and LAI data of MODIS correlate worse than the other data sources of these vegetation indices. MODIS evaporation has a very high correlation with the LAI of PROBA-V which is almost linear.

Conclusion and recommendations

The main focus of this report is on the performance of the evaporation models during the transition period of the Miombo woodlands. The evaporation models of Surface Energy Balance System (SEBS), Global Land Evaporation Amsterdam Model (GLEAM) and Terrestial ecosystem evapotranspiration model of MODIS (MOD16A2) are tested based on information from field observations, observation from the visual spectrum of Sentinel-2 images and the satellite products of three vegetation indices namely the Normalized Difference Vegetation Index (NDVI), the Normalized Difference Infrared Index (NDII) and the Leaf Area Index (LAI). Based on these sources, it can be concluded that MODIS is the most accurate evaporation model during the transition period. MODIS follows the trends of the vegetation indices and field observations the most which are probably due to the fact that it doesn't have some of the short-comings that GLEAM and SEBS display.

GLEAM is an evaporation model that responds really well to precipitation. The model, however, overestimates the water stress, the Miombo woodlands are likely to experience. This is mostly due to the fact that GLEAM uses a water balance model for the soil as a basis for water stress. Miombo trees, however, have the ability to store water in the tree trunks and more specific the Cambium. In addition, the soil module of GLEAM only reaches up to 250 cm while Miombo trees can possibly have access to deeper groundwater sources. Because of the fact, that the actual stress level for Miombo is lower, the Miombo trees can flush their leaves well before the first rains. Due to the wrong estimation of the stress levels, GLEAM is highly inaccurate in estimating the correct evaporation values during the transition period. It even seems to not respond to the transition period at all. It would be recommended to expand the root zone to cover the complete root zone of the Miombo trees and add a factor that accounts for the water storage inside the trees. This will reduce the stress factor and thus the overestimation of the water stress.

SEBS does respond to the transition period, although the model is a bit too early with its response. The model registers increasing evaporation values while the trees are shedding their leaves and this is therefore highly unlikely. In addition, SEBS unexpectedly drops its values again at the end of October. This is inaccurate, as this is the month in which most trees have already flushed their leaves. It is therefore unlikely that the evaporation values decrease. It is more likely that SEBS abrupt increase in July has to do with an increase in temperature. This increase could also be a consequence of slash and burn practices. The oscillations of SEBS is in the period in which slash and burn practices take place. It is recommended to research this matter further to understand why SEBS is oscillating only around this period of the year.

SEBS is also very vulnerable to temperature increases as the net radiation, the soil heat flux and the sensible heat flux are largely based on the temperature flux. I would advise the model to have a more diverse input so that temperature fluctuations have less of an impact on the end product. In addition to the influence of the fires, the daylight hours could also lead to a slight increase in temperature as it also increases the amount of solar radiation. It, however, does not explain the decrease at the end of October. Moreover, SEBS is based on the contrast between the dry and wet limit and therefore, similar to GLEAM can be inaccurate in the dry season as the model assumes that there is no evaporation at the dry limit. This while, the trees could store water in their stems and thus still evaporate. All in all, the model does not react accurately to the transition period.

As MODIS does not react only to precipitation and also has no abrupt and contradicting trends, this model has the trends which are likely a good representation of the actual evaporation values. This is probably due to the fact that MODIS calculates all the different evaporation types such as interception, transpiration and soil evaporation. Nevertheless, MODIS is has a few disadvantages such as the fact that it is an average value over 8 days which means, that the daily values are unknown and daily fluctuations are missed. The LAI input is based on MODIS input, I recommend using LAI PROBA-V input instead of MODIS LAI, as the difference between the two is very small and the PROBA-V has daily values. Moreover, Especially in November and December, MODIS is inaccurate. The transition period which happens before the first rains in November is, however,

accurately described and as this is the main focus of the report MODIS is seen as the most accurate evaporation model for the transition period. Although MODIS can still improve when it comes to fluctuations and the rainy season.

The evaporation models are based on vegetation indices among other things. Because of this, the vegetation outputs of several satellite products are studied. Three vegetation indices are chosen. First of all, the most commonly used one NDVI which is a good indicator of photosynthesis and primary production. The NDVI is compared to the NDII as this index should be better when indicating water stress due to its sensitivity to water and lastly the LAI, which estimates the amount of leaves. Comparing these vegetation indices shows that the NDVI and NDII output are quite similar except for the timing of the trough which is early and longer for the NDII than for the NDVI. Instead of only low values in September, the NDII already showed lower values in August. According to literature, the field observation, and Sentinel-2 images, the leaves start to fall in August and thus the NDII seems to have higher accuracy in regard to the timing of the leaf fall.

It is, however, not entirely certain that the leaves did fall in August and because of this nothing conclusive can be said. Additional satellite to ground research is necessary to be able to determine whether the timing of the NDVI or NDII is better for determining the start of the transition period in the Miombo woodlands. For the LAI, the decrease due to leaf abscission is less visible and more gradually. The LAI barely decreases after mid-June and it is unclear if this is correct or not. As the LAI also takes non-green leaves into account and young Brachystegia leaves have a reddish colour. The low decrease in LAI is, however, remarkable but could also mean that the leaf abscission and green-up happen around the same time. Because of this, the LAI index will only slightly decrease as the flushing or shedding of leaves will cancel each other out.

The vegetation indices follow the transition period quite well. GLEAM is the only model that does not use any of the vegetation indices but used the Vegetation Optical Depth (VOD). This is probably why GLEAM is very accurate when it comes to rain but does not follow the phenology stages that well. SEBS and MODIS both use the LAI as an input for their model. Therefore, the difference between SEBS and MODIS is model related and not based on the type of vegetation indices.

All in all, it is very hard to determine when the vegetation stages exactly took place due to the limiting time that could be spent in the field. In addition, satellite images cannot give a conclusive answer on the start of leaf abscission and the start of the green-up period which is especially due to the heterogeneity including the different grass to tree ratios throughout the woodlands. Moreover, it is hard to detect non-green leaves, which makes it difficult to accurately estimate the amount of leaves. Furthermore, it is hard to measure the vegetation changes through space as humans have a big impact on the state of the Miombo woodlands. Especially the slash and burn culture which burns large parts of the forest both in the early as in the late dry season.

The choice of evaporation model could, however, have a large impact on the output of your model as the annual difference of GLEAM and the other models are quite a lot as it is only 66% of SEBS and 71% MODIS. On the other hand the difference between MODIS and SEBS is on an annual basis not so big, these changes, however, in the transition period. As the vegetation and the field observation both agree with MODIS, I would recommend user's in these areas to use MODIS.

Bibliography

Astle, W., Phiri, P., Prince, S. (1997). A Dictionary of vernacular-scientific names of plants of the mid-Luangwa valley, Zambia. Kirkia, 16(2), 161-203. Retrieved from http://www.jstor.org/stable/23502321

AVHRR Surface Reflectance and Normalized Difference Vegetation Index (2018). Climate Algorithm Theoretical Basis Document, NOAA Climate Data Record Program CDRP-ATBD-0459 Rev. 2. Retrieved from http://www.ncdc.noaa.gov/cdr/operationalcdrs.html

Baret, F., Weiss, M., Verger, A. and Smets, B. (2013). ATBD for LAI, FAPAR and FCOVER from PROBA-V products at 300m resolution (GEOV3). IMAGINES_RP2.1_ATB-LAI300m, Issue 1.73. EC Proposal Reference N° FP7-311766. Retrieved from: https://land.copernicus.eu/global/sites/cgls.vito.be/files/products/ImagineS_RP2.1_ATBD-LAI300m_I1.73.pdf [Accessed at 4th of February 2020]

Borchert, R. And Rivera, G. (2001). Photoperiodic control of seasonal development and dormancy in tropical stem-succulent trees. Tree Physiology, 21, 213-221

Chidumayo, E.N. (1987). Species structure in Zambian Miombo woodland. Journal of Tropical Ecology 3: 109-118.

Chidumayo, E.N. (1992). The utilization and status of dambos in southern Africa: A Zambian case study. https://books.google.ch/ [Accessed at 16th of November 2019]

Chidumayo, E. and Frost, P. (1996). Population biology of Miombo trees. In: B. Campbell (ed.) The Miombo in Transition: Woodlands and Welfare in Africa, pp. 59-71. Centre for International Forestry Research, Bogor, Indonesia.

Chidumayo, E. (2001). Climate and Phenology of Savanna Vegetation in Southern Africa. Journal of Vegetation Science, 12, 347-354. DOI: 10.2307/3236848

Didan, K. (2015). MOD13Q1 MODIS/Terra Vegetation Indices 16-Day L3 Global 250m SIN Grid V006. NASA EOSDIS Land Processes DAAC. Retrieved from https://doi.org/10.5067/MODIS/MOD13Q1.006 { [Accessed at 14th of October 2019]

Didan, K., Munoz, A.B., Solano, R., Huete, A. (2015). MODIS Vegetation Index User's Guide (MOD13 Series). Version 3 Collection 6

Fang, H., Baret, F. Plummer, S. and Schaepman-Strub, G. (2019). An overview of global Leaf Area Index (LAI): Methods, Products, Validation, and Applications. https://doi.org/10.1029/2018RG000608

FAO-UN – AGLW. (2000). Inland water bodies in Africa. http://www.fao.org/geonetwork/srv/en/main.home

Frenken, K., and Faurès J. (1997). Irrigation potential in Africa: A basin approach. FAO Land and Water Bull. 4. Available at: http://www.fao.org/3/W4347E/W4347E00.htm [Accessed 18th of September 2018]

Frost, P. (1996). The ecology of miombo woodlands. In: B. Campbell (ed.) The Miombo in Transition: Woodlands and Welfare in Africa, pp. 11-57. Centre for International Forestry Research, Bogor, Indonesia.

Gerrits, A.M.J. (2010). The role of interception in the hydrological cycle. http://resolver.tudelft.nl/uuid:7dd2523b-2169-4e7e-992c-365d2294d02e

Gumbo, D.J., Dumas-Johansen, M., Muir, G., Boerstler, F., Xia, Z. (2018). Sustainable management of Miombo woodlands – Food security, nutrition and wood energy. Rome, Food and Agriculture Organization of the United Nations.

Hachigonta, S. And Reason, C. J. C. (2006). Interannual variability in dry and wet spell characteristics over Zambia. Climate Research Vol. 32: 49-62.

Higgins, S. I., Delgado-Cartay, M. D., February, E.C. and Combrink, H.J. (2011). Is there a temporal niche separation in the leaf phenology of savanna trees and grasses? Journal of Biogeography, 38, 2165-2175.

Ji,L., Zhang,L., Wylies, B.K., Rover, J. (2011). On the terminology of the spectral vegetation index (NIR – SWIR)/(NIR+SWIR). International Journal of Remote Sensing Vol. 32, No. 21, 6901-6909

JICA (2010). The study for power system development master plan in Zambia: final report. Japan International Cooperartion Agency: Chubu Electric Power Co., Inc. http://open_jicareport.jica.go.jp/640/640/640_533_11989118.html

Kaykeya, M. and Sugiyama, Y. (1985). Citemene, Finger Millet and Bemba Culture: A Socio-ecological Study of Slash-and-burn Cultivation in Northeastern Zambia. African Study Monographs. Supplementary Issue 4: 1-24

Kinyanjui, M. J. (2011). NDVI-based vegetation monitoring in Mau forest complex, Kenya. African Journal of Ecology, 49, 165-174.

Knyazikhin, Y., Glassy, J., Privette, L., Tian, Y., Lotsch, A., Zhang, Y., Wang, Y., Morisette, J. T., Votava, P., Myneni, R.B., Nemani, R.R., Running, S.W. (1999). MODIS Leaf Area Index (LAI) and Fraction of Photosynthetically Active Radiation Absorbed by Vegetation (FPAR) Product (MOD15) Algorithm Theoretical Basis. Document, http://eospso.gsfc.nasa.gov/atbd/modistables.html

LAND COVER CLASSIFICATION SYSTEM. (2000). Retrieved 12 November 2019, from http://www.fao.org/3/x0596e/X0596e01n.htm

Lehner, B., Verdin, K., Jarvis, A. (2006). HydroSHEDS Technical Documentation. World Wildlife Fund US, Washington, DC. Available at http://hydrosheds.cr.usgs.gov.

Li, Z., Tang, R., Wan, Z., Bi, Y., Zhou, C. Tang, B. Yan, G. and Zhang, X. (2009). A Review of Current Methodlogies for Regional Evapotranspiration Estimation from Remotely Sensed Data. Sensors (Basel). 2009; 9(5):3801-53. doi: 10.3390/s90503801

Mapcruzin (2019). Zambia Country, city, region, boundaries GIS Shapefile Map Layers. Retrieved from https://mapcruzin.com/free-zambia-country-city-place-gis-shapefiles.htm [Accessed on 15th of November 2019]

Martens, B., Miralles, D., Lievens, H., Fernández-Prieto, D. Verhoest, N.E.C. (2016). Imporving terrestrial evaporation estimates over continental Australia through assimilation of SMOS soil moisture. International Journal of Applied Earth Observation and Geoinformation, 48, 146-162

Martens, B., Miralles, D.G., Lievens, H., van der Schalie, R., de Jeu, R.A.M., Fernández-Prieto, D., Beck, H.E., Dorigo, W.A., and Verhoest, N.E.C. (2017). GLEAM v3: satellite-based land evaporation and root-zone soil moisture, Geoscientific Model Development, 10, 1903–1925.

Miralles, D. G. (2011a). Evaporation in the global water cycle: Analysing land evaporation using satellite observations https://www.researchgate.net/publication/233388624

Miralles, D.G., Holmes, T.R.H., de Jeu, R.A.M., Gash, J.H., Meesters, A.G.C.A., Dolman, A.J. (2011b). Global land-surface evaporation estimated from satellite-based observations. Hydrology and Earth System Sciences, 15, 453-469, doi: 10.5194/hess-15-453-2011

Mpika Weather station (2019). Precipitation data from the Mpika Weather Station provided by Makawa Haggai and Charles Silwenga.

Myneni, R., Knyazikhin, Y., Park, T. (2015). MCD15A2H MODIS/Terra+Aqua Leaf Area Index/FPAR 8-day L4 Global 500m SIN Grid V006. NASA EOSDIS Land Processes DAAC. Accessed 2019-10-14 from https://doi.org/10.5067/MODIS/MCD15A2H.006. Accessed October 14, 2019.

Myneni, R., Knyazkhin, Y. (2018). VIIRS/NPP Leaf Area Index/FPAR 8-Day L4 Global 500m SIN Grid V001. NASA EOSDIS Land Processes DAAC. Accessed 2019-10-14 from https://doi.org/10.5067/VIIRS/VNP15A2H.001. Accessed October 14, 2019.

Mu, Q., Zhao, M. and Running, S.W. (2013). MODIS Global Terrestrial Evapotranspiration (ET) Product (NASA MOD16A2/A3), Algorithm Theoretical Basis Document, Collection 5

National Aeronautics and Space Administration, Science Mission Directorate. (2010). Reflected Near-Infrared Waves. Retrieved *[insert date - e.g. August 10, 2016]*, from NASA Science website: http://science.nasa.gov/ems/08_nearinfraredwaves

Nkengurutse, J., Houmy, N., Mansouri, F., Ben Moumen, A., Serghini Caid, H. and Khalid A. (2016). Prelimitary Chemical Characterization of Amashindwi (Anisophyllea boehmii Engl.) Kernels and Kernel oi. J. Mater. Environ. Sci. 7 (6)

Olson, D. M., Dinerstein, E., Wikramanayake, E. D., Burgess, N. D., Powell, G. V. N., Underwood, E. C., D'Amico, J. A., Itoua, I., Strand, H. E., Morrison, J. C., Loucks, C. J., Allnutt, T. F., Ricketts, T. H., Kura, Y., Lamoreux, J. F., Wettengel, W. W., Hedao, P., Kassem, K. R. (2001). Terrestrial ecoregions of the world: a new map of life on Earth. Bioscience 51(11):933-938.

Orwa C, A Mutua, Kindt R , Jamnadass R, S Anthony. (2009). Agroforestree Database:a tree reference and selection guide version 4.0 (http://www.worldagroforestry.org/sites/treedbs/treedatabases.asp)

Priestley, J. H. C. and Taylor, J. (1972). On the assessment of surface heatflux and evaporation using large-scale parameters, Mon. WeatherRev., 100, 81–92

Richter, H.V. & Cumming G.S. (2005). Food availability and annual migration of the straw-colored fruit bat (Eidolon helvum). Journal of Zoology v268 n1 (20051219): 35-44. https://zslpublications-onlinelibrary-wiley-com.tudelft.idm.oclc.org/doi/epdf/10.1111/j.1469-7998.2005.00020.x

Running, S., Mu, Q., Zhao, M. (2017). MOD16A2 MODIS/Terra Net Evapotranspiration 8-Day L4 Global 500m SIN Grid V006. NASA EOSDIS Land Processes DAAC. Accessed 2019-10-14 from https://doi.org/10.5067/MODIS/MOD16A2.006. Accessed October 14, 2019.

Running, S.W., Mu, Q., Zhao, M., Moreno, A. (2018) User's Guide MODIS Global Terrestrial Evapotranspiration (ET) Product (NASA MOD16A2A3). NASA Earth Observing System MODIS Land Algorithm. Version 1.6 for Collection 6

Ryan, C.M., William, M., Grace, J., Woollen, E., Lehmann, C.E.R. (2017). Pre-rain green-up in ubiquitous across southern tropical Africa: implications for temporal niche separation and model representation, New Phytologist 213:625-633 doi:10.1111/nph.14262

Simute S., Phiri C.L. & Tengnäs B. (1998). Agroforestry Extension Manual for Eastern Zambia. Nairobi, Kenya: Regional Land Management Unit (RELMA) Accessed online X-2016 via http://www.worldagroforestry.org/usefultrees

Sriwongsitanon, N., Gao, H., Savenije, H. H. G., Maekan, E., Saengsawang, S., and Thianpopirug, S. (2016). Comparing the Normalized Difference Infrared Index (NDII) with root zone storage in a lumped conceptual model, Hydrol. Earth Syst. Sci., 20, 3361–3377, https://doi.org/10.5194/hess-20-3361-2016

Su, Z. (2001). A Surface Energy Balance System (SEBS) for estimation of turbulent heat fluxes from point to continental scale. Advanced Earth Observation – Land Surface Climate

Su, Z. (2002). The Surface Energy Balance System (SEBS) for estimation of turbulent heat fluxes, Hydrol. Earth Syst. Sci., 6, 85–100, https://doi.org/10.5194/hess-6-85-2002

Szilagyi, J., Rundquist, D.C. and Gosselin C. (1998). NDVI relationship to monthly evaporation, Geophysical research letters, vol. 25, No, 10, 1753-1756

Tian, F., Wigneron, J.P., Ciais, P., Chave, J., Ogée, J., Peñuelas, J., Ræbild, A., Domec, J.C., Tong, X. Brandt, M. Mialon, A., Rodriguez=Fernandez, N. Tagesson, T., Al-Yaari, A., Kerr, Y., Chen, C., Myneni, R.B., Zhang, W., Ardö, J and Fensholt, R. (2018). Coupling of ecosystem-scale plant water storage and leaf phenology observed by satellite. Nature Ecology & Evolution 2, 8: 1428-35. https://doi.org/10.1038/s41559-018-0630-3

Valente, F., David, J.S., Gash, J.H.C. (1997). Modelling interception loss for two sparse eucalypt and pine forests in central Portugal using reformulated Rutter and Gash analytical models. Journal of Hydrology, 190, 141-162

Vegetation and EMR. (2019). Retrieved from http://gsp.humboldt.edu/OLM/Courses/GSP_216_Online/lesson2-1/vegetation.html [Accessed on 18th of October 2019]

Vermote, E. (2015). MOD09A1 MODIS/Terra Surface Reflectance 8-Day L3 Global 500m SIN Grid V006. NASA EOSDIS Land Processes DAAC. Accessed 2020-02-05 from https://doi.org/10.5067/MODIS/MOD09A1.006. [Accessed on 5th of February 2020]

Vinya, R., Malhi, Y., Brown, N.D., Fisher, J. B., Brodribb, T. and Aragão, L.E.O.C. (2018). Seasonal changes in plant-water relations influcne patterns of leaf display in Miombo woodlands: evidence of water conservative strategies. Tree Physiology 39, 104-112. doi: 10.1093/treephys/tpy062

Von der Heyden, C. J., New, M. G. (2003). The role of a dambo in the hydrology of a catchment and theriver network downstream. Hydrology and Earth System Sciences Discussions, European GeosciencesUnion. 7 (3), pp.339-357. hal-00304785

White, F. (1983). The Vegetation of Africa: A descriptive memoir to accompany the UNESCO/AETFAT/UNSO vegetation map of Africa. UNESCO, Paris. doi: 10.5281/zenodo.293797

Wilding, I. G. P. (1965). Investigation of the secondary dispersion of Nickel in Rhodesia and Zambia. PHD thesis at the Royal School of Mines Imperial College

Wilson, N. R. and Norman, L. M. (2018) Analysis of vegetation recovery surrounding a restored wetland using the normalized difference infrared index (NDII) and normalized difference vegetation index (NDVI), International Journal of Remote Sensing, 39:10, 3243-3274, DOI: 10.1080/01431161.2018.1437297

World Bank (2010). The Zambezi river basin : a multi-sector investment opportunities analysis (Vol. 3) : State of the Basin (English). Washington, DC: World Bank. http://documents.worldbank.org/curated/en/938311468202138918/State-of-the-Basin [Accessed 18th of September 2018]

Appendix 1 – Sentinel band values

In the table below trends in values of the visible band are shown and groups are made based on the values between 10-20, 100-110 etc. The Red band value trend shows the most similar trend to the trend observed in the field work. Because of this, the red band is taken as an indication of the seasons.

	Green		Blue		Red	
	LUM	LTM	LUM	LTM	LUM	LTM
12-mei	118		58		107	
27-mei		118		60		107
30-mei						
1-jun						
11-jun	117	117	62	61	108	106
16-jun		117		62		108
21-jun	116	116	64	63	109	107
1-jul		116		63		107
21-jul		119		67		112
26-jul	115	115	64	67	108	109
31-jul	111	114	66	68	108	108
5-aug	115	116	65	64	111	109
10-aug	114	113	70	69	113	114
15-aug	119	116	70	70	117	117
20-aug	118	120	75	76	121	121
25-aug	120		77		123	
30-aug	123	124	74	76	121	125
4-sep	125	127	76	77	127	127
9-sep	124	123	82	81	123	122
14-sep	128	127	83	83	125	126
19-sep	134	134	84	84	132	132
24-sep	136	136	85	86	132	134
29-sep	135	134	90	90	132	133
9-okt	139	141	83	84	134	133
14-okt	144		84		134	
19-okt	145	145	81	83	133	131
24-okt		143		75		132
29-okt	141		78		131	
13-nov	142	142	78	76	130	130
18-nov	142	143	76	74	130	128
8-dec	145	144	75	73	128	127
13-dec	150		66		121	
18-dec	145	142	79	83	116	114

Table 12 Sentinel Visible bands outputs

Appendix 2 - All NDVI products

This graph also includes the oscillating AVHRR NOAA product and all the MODIS products.

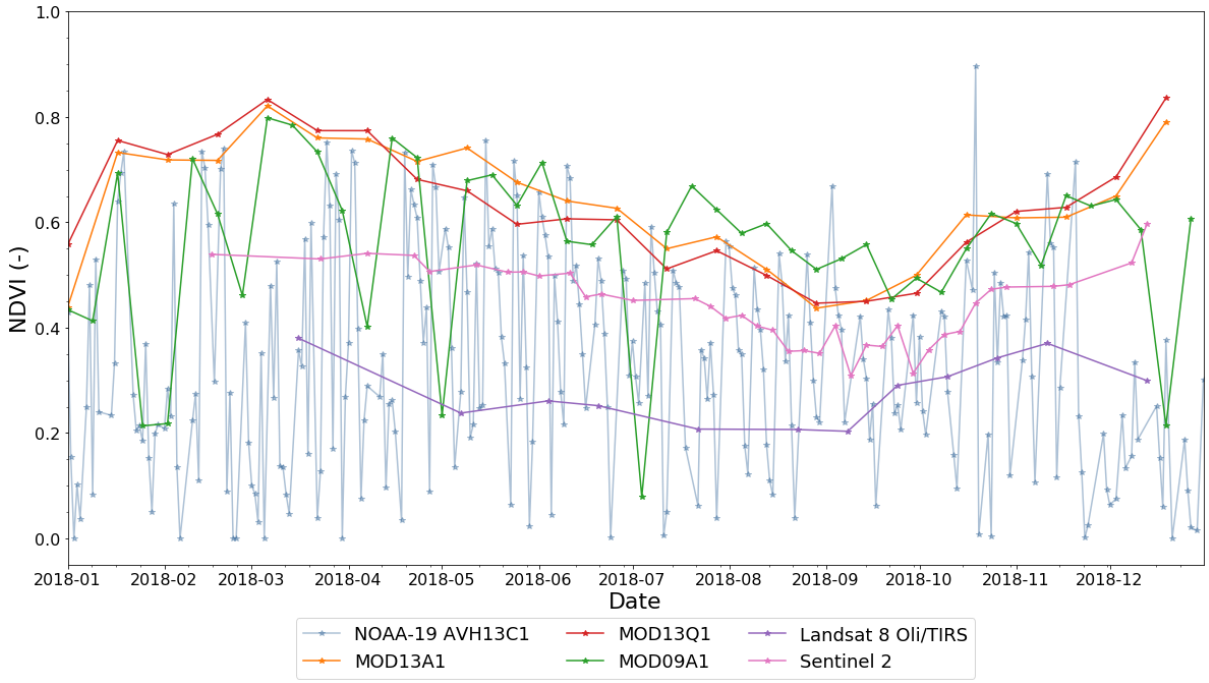

Figure 20 All NDVI products (AVHRR Surface Reflectance and Normalized Difference Vegetation Index, 2018; Didan, 2015; Myeni and Knyazikhin, 2015; Vermote, 2015; Contains modified information from Landsat-8 images courtesy of the U.S. Geological Survey and Copernicus Service information [2018])

Appendix 3 – Bemba to scientific names

Local name to scientific name translation

Scientific name	Bemba name
Anisophyllea boehmii[2,5]	(U)mufungo
Bauhinia petersenia[2]	Umunpo → Umupo
Brachystegia floribunda[5]	(U)mbuta/(U)musompa
Brachystegia longifolia[6,7]	(U)muwombo
Brachystegia spiciformis[1,2,3]	(U)muputu
Cryptosepalum exfoliatum spp. Pseudotaxus[2]	(U)mukuwe
Dichrostacys cinerea[1]	Katenge
Faurea saligna[1,2,3,5]	Saninga
Julbernardia paniculata[2,3]	(U)mutundo
Lannea discolour[2]	(Na)kabumbu
Onocoba spinosa[2]	(U)musongwa → (U)musangwa
Parinari curatelifolia[1.2,3,4,5]	Mupundu
Pericopsis angolensis (Afromosia angolensis)[3,5]	(U)mubanga
Swartzia madagascariensis[2,3]	Ndale (U)mulundu
Uapaca kirkiana[1,2,4,5]	Musuku
Uapaca sansibarica[4]	Swebya
Vitex doniana[3]	Umufishamano → Mfishameno
Unidentified	Umupolombwe Ingasa

Table 13 Tree classification based on local language (Bemba) converted to scientific names. The references are based on numbers behind the scientific name: 1. Orwa et al. (2009), 2. JICA (2010), 3. Astle et al. (1997), 4. Richter and Cumming (2005), 5. Kakeya & Sugiyama (1985), 6. Wilding (1965) and 7. Forestry Deparment (2016)

Appendix 4 – Spatial and Temporal resolution

NDVI	Spatial	Temporal (* in cloud free conditions)	NIR wavelength (nm)	RED band wavelength (nm)
NOAA-19	0.05° latitude-longitude grid (± 5.5 by 5.5 km)	Daily	720-1000	580-680
Landsat 8	30 m	Every 16 days	851-879	636-673
Sentinel-2	10 m	Every 5 days	763-908	646-685
MOD13A1	500 m	Every 16 days	841-876	620-670
MOD13Q1	250 m	Every 16 days	841-876	620-670
MYD13A1	500 m	Every 16 days	841-876	620-670
MOD09A1	500 m	Every 8 days	841-876	620-670

Table 14 NDVI spatial and temporal resolution

NDII	Spatial	Temporal (* in cloud free conditions)	NIR wavelength (nm)	SWIR band wavelength (nm)
Landsat 8	30 m	Every 16 days	851-879	1560-1660
Sentinel-2	20 m	Every 5 days	763-908	1540-1685
MOD09A1	500 m	Every 16 days	841-876	1628-1652

Table 15 NDII spatial and temporal resolution

Model	Spatial	Temporal (* in cloud free conditions)
MCD15A2H	500	Every 8 days
MCD15A3H	500	Every 4 day
PROBA-V	300	Daily

Table 16 LAI spatial and temporal resolution.

Model	Blue wavelength (nm)	Red wavelength (nm)	NIR wavelength (nm)	SWIR band wavelength (nm)
MCD15A2H	459-479	620-670	841-876	1628-1652
MCD15A3H	459-479	620-670	841-876	1628-1652
PROBA-V	447-493	610-690	777-897	1570-1650

Table 17 bands LAI

AVHRR Surface Reflectance and Normalized Difference Vegetation Index, 2018
Contains modified information from Landsat-8 images courtesy of the U.S. Geological Survey [2018]
Contains modified information from Sentinel and PROBA-V, Copernicus Service information [2018]

Appendix 5 – Correlation of all the satellite products

Correlations of the NDVI, NDII and LAI products with products of the same vegetation index.

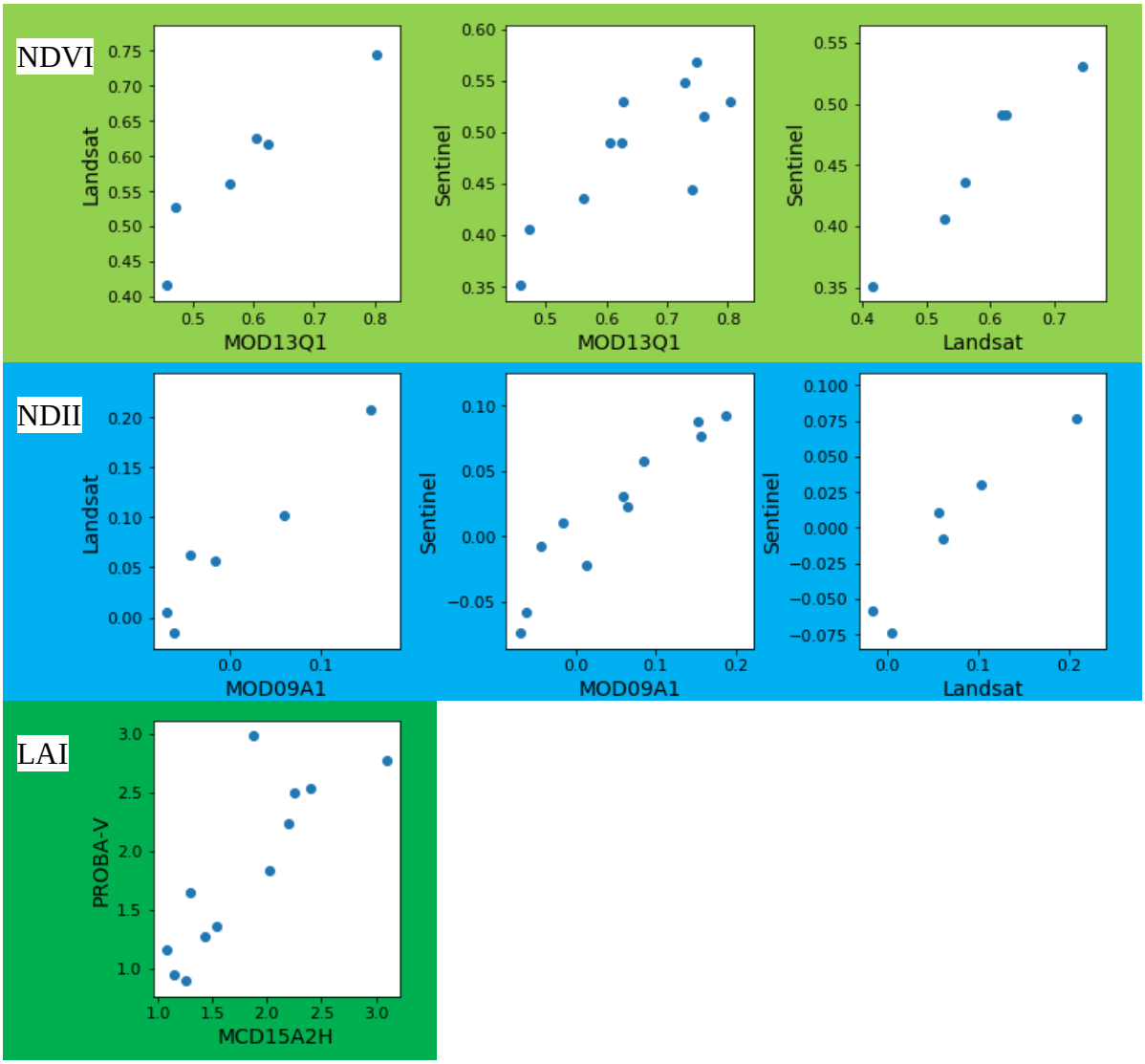

2018	Column 1		Column 2		Column 3	
	Pearson	p-value	Pearson	p-value	Pearson	p-value
NDVI	0.947	4.1E-03	0.895	2.0E-04	0.976	8.5E-04
NDII	0.965	1.8E-03	0.946	1.028	0.959	3.8E-03
LAI	0.839	6.5E-04				

Correlations between SEBS and the vegetation indices (except landsat since there were no common daily points)

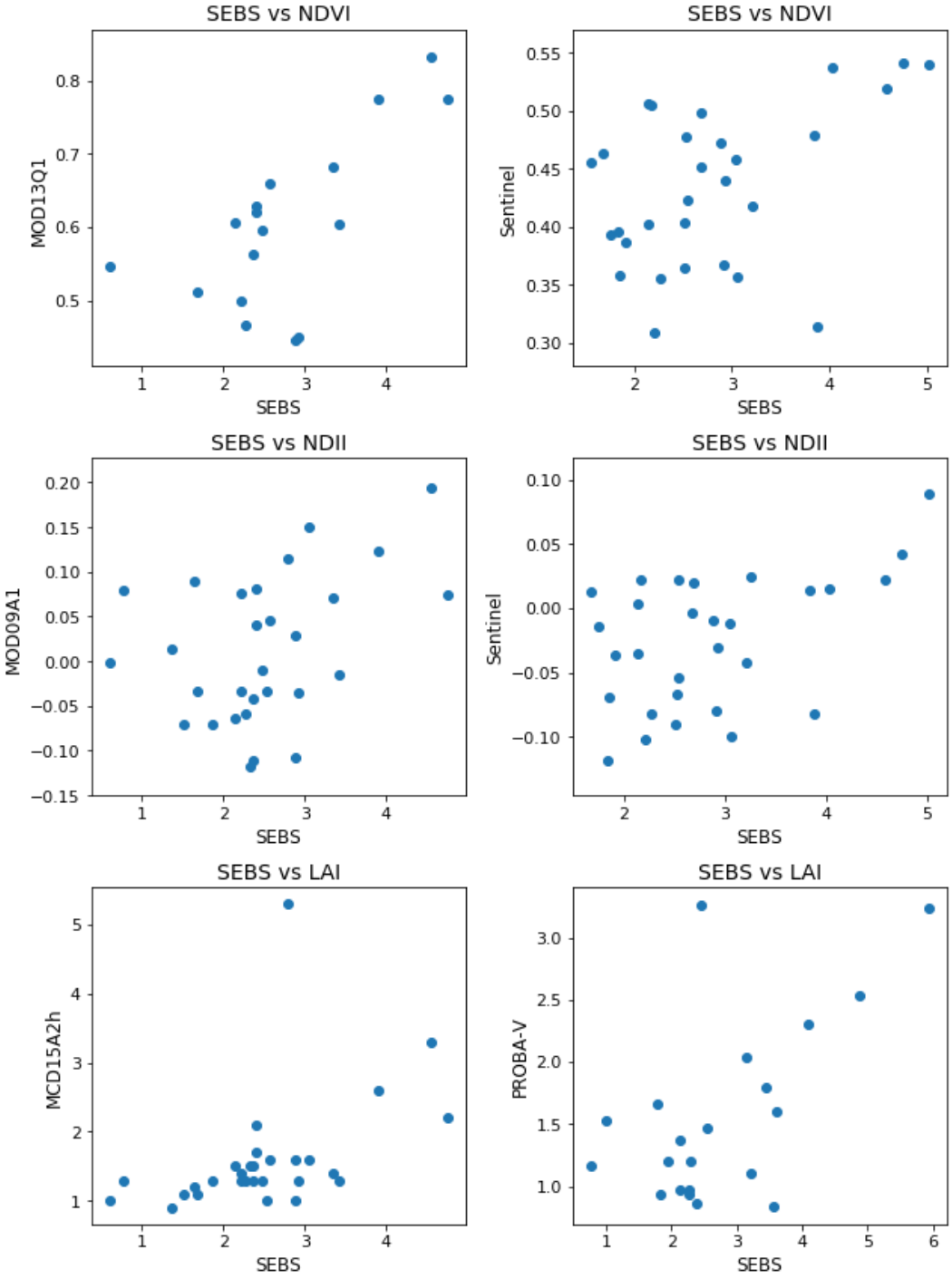

2018	Column 1		Column 2	
	Pearson	p-value	Pearson	p-value
NDVI	**0.689**	1.1E-3	0.508	2.6E-3
NDII	0.380	0.035	0.535	1.6E-3
LAI	0.450	0.011	**0.657**	9.0E-4

*Zero points between SEBS and Landsat

Correlations between GLEAM and the vegetation indices

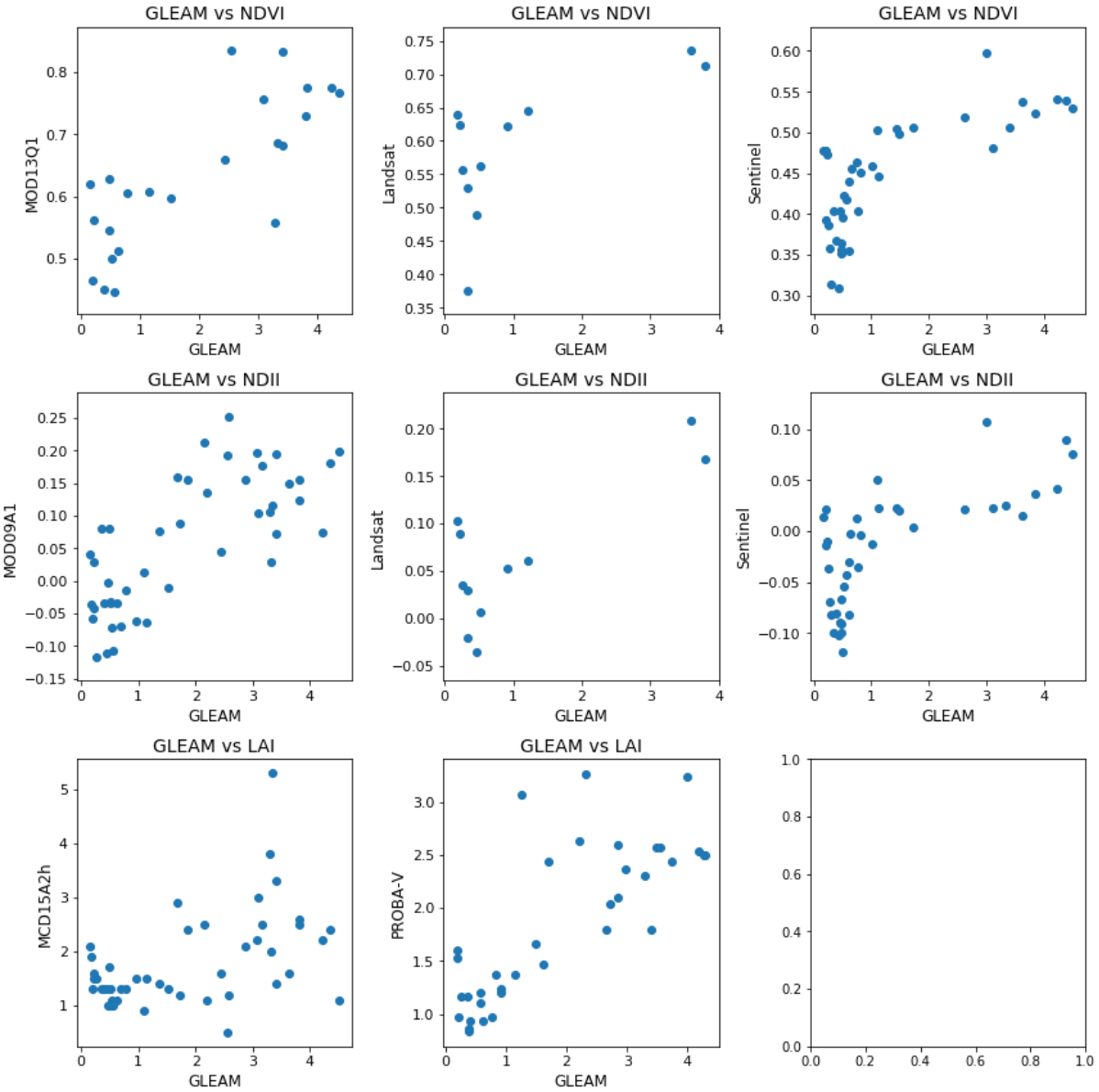

	Column 1		Column 2		Column 3	
2018	Pearson	p-value	Pearson	p-value	Pearson	p-value
NDVI	0.796	5.6E-6	0.686	0.020	0.746	7.7E-8
NDII	0.756	2.7E-9	0.796	3.4E-3	0.709	6.2E-7
LAI	0.489	5.6E-4	0.783	1.7E-8	X	X

Correlations between MODIS and the vegetation indices

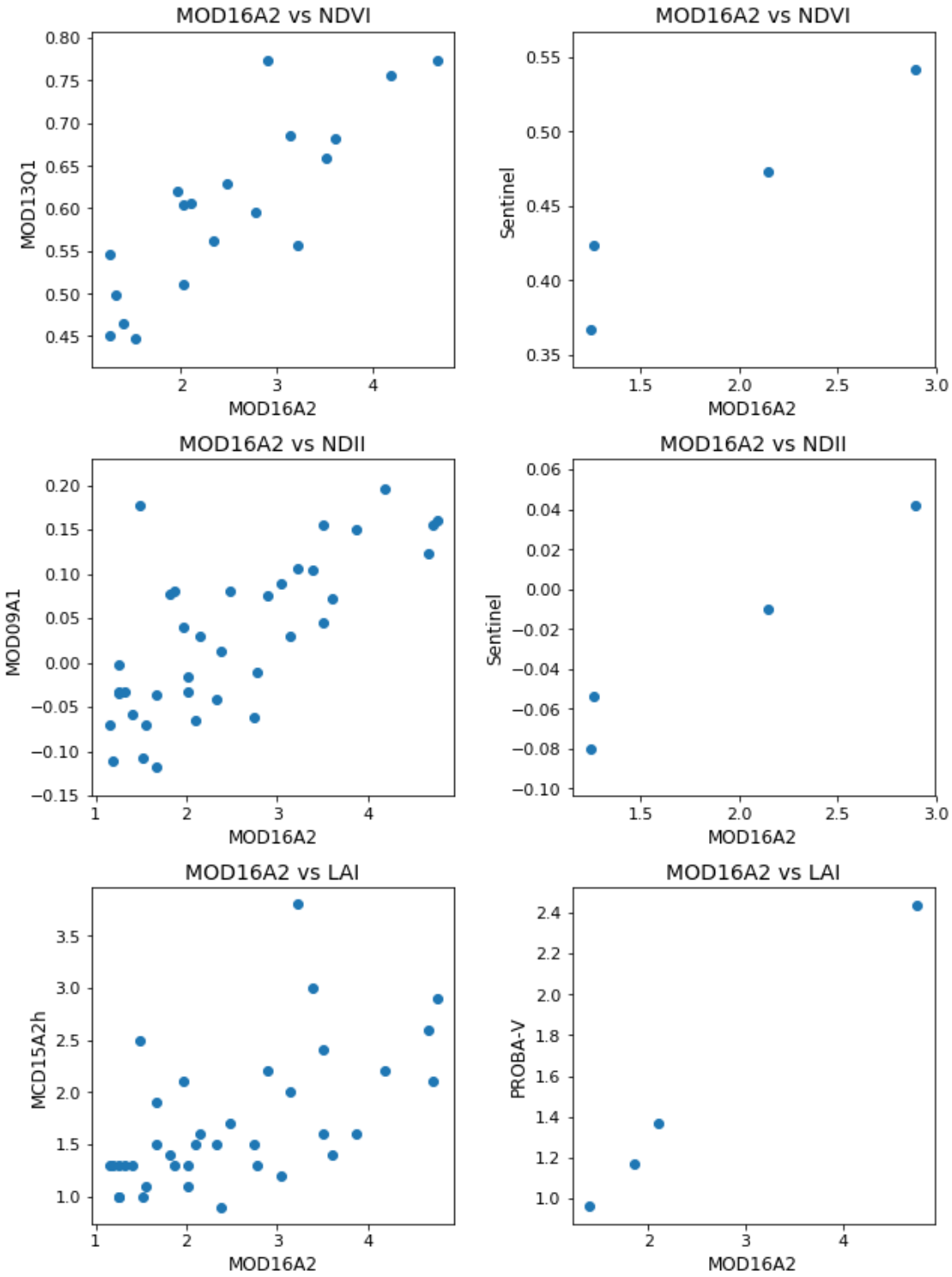

	Column 1		Column 2	
2018	Pearson	p-value	Pearson	p-value
NDVI	**0.853**	4.460	0.942	0.058
NDII	0.738	1.6E-8	0.963	0.037
LAI	0.572	6.1E-5	**0.999**	1.5E-3

Correlations from evaporation products

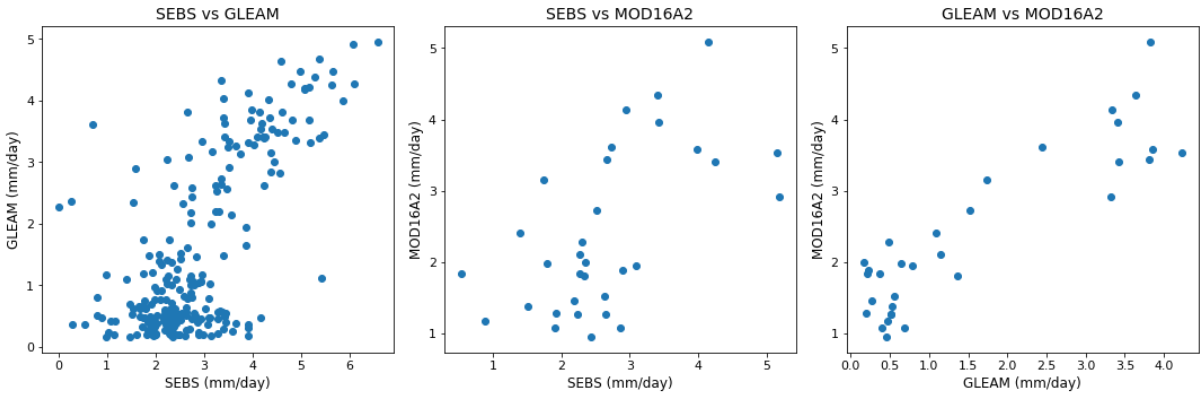

	SEBS vs GLEAM		SEBS vs MOD16		GLEAM vs MOD16	
2018	Pearson	p-value	Pearson	p-value	Pearson	p-value
Evaporation	0.698	3.80E-36	0.593	3.5E-4	0.897	3.7E-12